An admissibility and asymptotic preserving scheme for systems of conservation laws with source term on 2D unstructured meshes with high-order MOOD reconstruction

Florian Blachère, Rodolphe Turpault

An admissibility and asymptotic preserving scheme for systems of conservation laws with source term on 2D unstructured meshes with high-order MOOD reconstruction

F. Blachère[a,b,*], R. Turpault[c]

[a] *Laboratoire de Mathématiques Jean Leray, Université de Nantes, 2 rue de la Houssinière 44322 Nantes Cedex 3, France.*
[b] *Laboratoire de Mathématiques de Versailles, Université de Versailles Saint-Quentin-en-Yvelines, 45 Avenue des États-Unis, 78035 Versailles Cedex, France.*
[c] *Institut de Mathématiques de Bordeaux, Bordeaux-INP, 351 cours de la Libération Bât A33, 33405 Talence Cedex, France.*

Abstract

The aim of this work is to design an explicit finite volume scheme with high-order MOOD reconstruction for specific systems of conservation laws with stiff source terms which degenerate into diffusion equations. We propose a general framework to design an asymptotic preserving scheme that is stable and consistent under a classical hyperbolic CFL condition in both hyperbolic and diffusive regimes for any 2D unstructured mesh. Moreover, the developed scheme also preserves the set of admissible states, which is mandatory to conserve physical solutions in stiff configurations. This construction is achieved by using a non-linear scheme as a target scheme for the limit diffusion equation, which gives the form of the global scheme for the full system. The high-order polynomial reconstructions allow to improve the accuracy of the scheme without getting a full high-order scheme. Numerical results are provided to validate the scheme in every regime.

Keywords: asymptotic-preserving schemes, finite volumes schemes, hyperbolic systems of conservation laws with source terms, MOOD.

1. Introduction

In this work we study the numerical approximation of systems of conservation laws with stiff source terms, which can be written in the following formalism:

$$\partial_t \mathbf{U} + \operatorname{div}(\mathbf{F}(\mathbf{U})) = \gamma(\mathbf{U})(\mathbf{R}(\mathbf{U}) - \mathbf{U}), \tag{1.1}$$

where the vector of conservative variable $\mathbf{U}$ is in $\mathcal{A} \subset \mathbb{R}^n$ the set of admissible states. The source term is composed of γ a positive function that controls its stiffness and $\mathbf{R}(\mathbf{U}) \in \mathcal{A}$. The homogeneous hyperbolic system associated to (1.1) is:

$$\partial_t \mathbf{U} + \operatorname{div}(\mathbf{F}(\mathbf{U})) = 0, \tag{1.2}$$

*Corresponding author

with $\mathbf{F}$ the hyperbolic physical flux. The compatibility conditions from [5] are assumed to be fulfilled so that when $\gamma(\mathbf{U})t \to \infty$ the system (1.1) degenerates into a diffusion equation:

$$\partial_t u - \operatorname{div}\big(D(u)\nabla u\big) = 0, \tag{1.3}$$

where $u \in \mathbb{R}$ is linked to $\mathbf{U}$, and D is positive function.

The key point of this work is to construct high-order schemes which extend the 1D asymptotic preserving (AP for short) scheme designed in [7] and the one for 2D unstructured meshes from [9]. This extension to high-order has to be done without losing the AP property of the first-order schemes.

The AP property will be considered in the sense of Jin [40] that is Figure 1 holds with uniform bounds on the parameters in terms of γt (eg. the CFL condition).

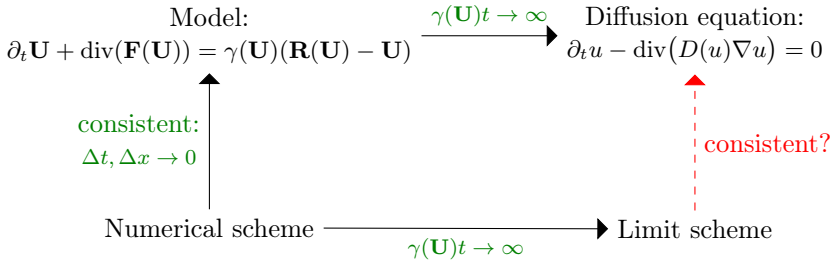

Figure 1: Aim of an AP scheme

Throughout this paper, the isentropic Euler model with friction is used as an example:

$$\mathbf{U} = \begin{pmatrix} \rho \\ \rho\mathbf{u} \end{pmatrix}, \mathbf{F}(\mathbf{U}) = \begin{pmatrix} (\rho\mathbf{u})^T \\ \rho\mathbf{u} \otimes \mathbf{u} + p\mathbf{I} \end{pmatrix}, \mathbf{R}(\mathbf{U}) = \begin{pmatrix} \rho \\ 0 \end{pmatrix}, \tag{1.4}$$

where $\gamma(\mathbf{U}) = \kappa(\rho) > 0$ is the friction coefficient and $p(\rho)$ a pressure law with $p'(\rho) > 0$. For all the test cases we choose $p(\rho) = \rho^{1.4}$. The set of admissible states of this model is, in 2D:

$$\mathcal{A} = \{\mathbf{U} = (\rho, \rho\mathbf{u})^T \in \mathbb{R}^3 / \rho > 0\}.$$

When $\kappa t \to \infty$, the system degenerates into the following diffusion equation (see [47, 33, 36, 5] for a rigorous proof):

$$\partial_t \rho - \operatorname{div}\left(\frac{p'(\rho)}{\kappa(\rho)}\nabla\rho\right) = 0. \tag{1.5}$$

Various others systems enter the framework of (1.1), including the P_1 model for radiative transfer [14] or the M_1 model [25, 7, 9]. Let us emphasize the fact that γ does indeed strongly depends on $\mathbf{U}$ in several applications. Hence, it is crucial to build a numerical scheme able to deal with this feature.

There is a strong interest in developing AP schemes in our context since the pioneer work of Gosse and Toscani [29]. This work has been generalised in [7] for all systems in our formalism (1.1) for the 1D case. Then, several works have been done to construct AP schemes in 2D, by using 1D techniques [26, 6, 9] or MPFA based schemes [13, 14, 15, 16]. The aim is now to develop high-order finite volume schemes for those systems, especially for 2D unstructured meshes. IMEX

methods [1] and (W)ENO discretizations [34, 45] has been used to get up to second and third-order schemes in [11, 10] for some 1D hyperbolic systems and kinetic equations. When dealing with kinetic equations one may also use projective integrations [43] or again IMEX time schemes with micro-macro decomposition and Discontinuous Galerkin [38] to construct high-order schemes, for instance. This list of techniques is not exhaustive and for more details about each method the reader is referred to the cited works and dereferences therein.

The content of this work is divided into two main parts: one for 1D schemes and another one for 2D schemes conducted on unstructured meshes. Inside each part, the first-order scheme is quickly recalled for the homogeneous hyperbolic system (1.2) then extended to high-order. Then, the construction of a scheme using high-order polynomial reconstruction of the MOOD method [19] is also done with the two AP schemes for the system with source term (1.1) in 1D and 2D. Besides, results are presented with reference solutions constructed in the appendices, and the convergence towards the diffusion limit is investigated.

2. Asymptotic preserving scheme in 1D

2.1. High-order scheme for the homogeneous system

First of all, let us recall the general framework for an explicit first-order 1D finite volume scheme for the homogeneous hyperbolic system (1.2):

$$\mathbf{U}_i^{n+1} = \mathbf{U}_i^n - \frac{\Delta t}{\Delta x}\left(\boldsymbol{\mathcal{F}}_{i+1/2} - \boldsymbol{\mathcal{F}}_{i-1/2}\right), \tag{2.1}$$

where the classical notations are used. Hence, when using uniform 1D meshes, a cell i is composed of a segment $[x_{i-1/2}; x_{i+1/2}]$, with a cell center located at $x_i := \frac{x_{i+1/2}+x_{i-1/2}}{2}$ and the space step is $\Delta x := x_{i+1/2} - x_{i-1/2}$.

In this scheme $\boldsymbol{\mathcal{F}}_{i+1/2} = \boldsymbol{\mathcal{F}}(\mathbf{U}_i, \mathbf{U}_{i+1})$ is a two points approximate Riemann solver such as Rusanov [48], HLL [35] or HLLC [57, 58, 3] for instance. This first-order scheme is consistent with the hyperbolic system (1.2), stable and conserves the set of admissible states $\mathcal{A}$ under a classical hyperbolic CFL condition:

$$\frac{\Delta t}{\Delta x}\max_i\left(|b^-_{i+1/2}|, |b^+_{i+1/2}|\right) \leq \frac{1}{2}, \tag{2.2}$$

where $b^+_{i+1/2}$ and $b^-_{i+1/2}$ are speeds respectively larger and smaller than all wave speeds at interface $x_{i+1/2}$.

In order to get a better accuracy, the extension of (2.1) to high-order is considered. In order to do so, different technique in the framework of the finite volume method can be used. For instance, MUSCL [59], ENO [34] or WENO [45, 39, 51] reconstructions can be set up. For space and time high-order methods it is also possible to use the ADER [56] or GRP [2] methods. We choose to use the MOOD method initially introduced in [19] and then extended and used in [22, 23, 4, 46, 12]. This choice has been made as the *a posteriori* paradigm is already used for the first-order scheme in 2D [9]. Besides, the MOOD method allows to easily reach very high-order scheme with a general formalism.

In this method the polynomial reconstruction of degree d of the solution on cell i is:

$$\widetilde{\mathbf{U}}_i^n(x) = \mathbf{U}_i^n + \sum_{\alpha=1}^{d} \boldsymbol{\mathcal{R}}_i^\alpha(\mathbf{U}^n)\left((x-x_i)^\alpha - \frac{1}{\Delta x}\int_i (x-x_i)^\alpha dx\right), \tag{2.3}$$

where $\boldsymbol{\mathcal{R}}_i^\alpha$ are the polynomial coefficients obtained by least-square interpolations, the reader is referred to [22] to see the details of this interpolation.

Remark 2.1. *The expression of the polynomial reconstruction (2.3) can be slightly simplified in 1D, but we keep this general expression to make easier the link with the 2D extension (4.3). Besides, we can easily see that the MOOD reconstruction preserves the mean values:* $\frac{1}{\Delta x}\int_i \widetilde{\mathbf{U}}_i^n(x)dx = \mathbf{U}_i^n$, *which is critical to obtain an order greater than two.*

The key point of the MOOD method is the *a posteriori* limitation, where the others methods *a priori* limit the polynomial reconstruction. Indeed, this paradigm (see Figure 2) consists in computing a candidate solution $\mathbf{U}^\star$ with an unlimited high-order scheme then check if this solution respects some criteria. If the solution is not acceptable (in the sense of the criteria chosen), then the degree of the polynomial reconstruction is locally decreased until the first-order scheme is reached. In order to end the loop, the last scheme of order one (known as the "parachute" scheme) has to satisfy all the criteria. Practically speaking, those checks need to be done at each stage of the Runge-Kutta time schemes, to ensure the validity of the solution during all the computations. This *a posteriori* limitation allows to reach a very high-order without complex modifications of the original scheme.

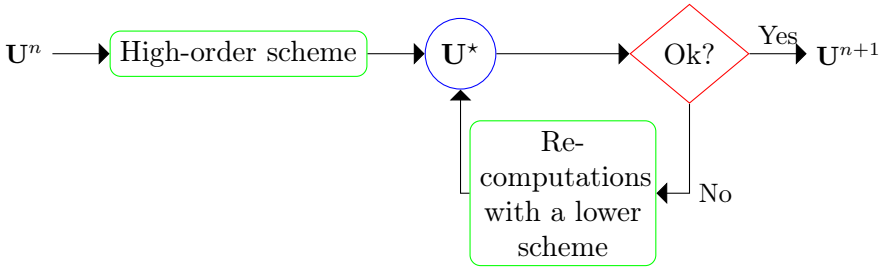

Figure 2: MOOD paradigm

For the sake of completeness, we recall the main limiters that may be used in the MOOD method:

- the Physically Admissible Detector (PAD) which detects if a solution is in the set of admissible states $\mathcal{A}$,
- the Discrete Maximum Principle (DMP) detector or the Extrema Detector (ED) introduced in [20], coupled with the u2 detector in order to eliminate spurious oscillations and keep smooth extrema,
- the entropic criterion developed in [4], to filter non-entropic solutions.

In this work, we mainly use the PAD limiter on the density when dealing with the isentropic Euler equations (1.4) and the DMP is only used for the last numerical test. For the linear systems studied (the Telegraph equations (3.1), the P1 model (5.2) or the transport equation (5.1)) the DMP limiter is sometimes used. When nothing is mentioned, no limiters are used in the MOOD loop.

With the MOOD paradigm, all the properties of the based scheme can be preserved if the proper tests are made during the *a posteriori* limitation. For instance, it can be proved that the high-order scheme preserves the set of admissible states $\mathcal{A}$ if the PAD criterion is used.

Using the high-order polynomial reconstruction (2.3), one can build the high-order version of the scheme for the homogeneous system in 1D (2.1):

$$\mathbf{U}_i^{n+1} = \mathbf{U}_i^n - \frac{\Delta t}{\Delta x}\left(\boldsymbol{\mathcal{F}}\left(\widetilde{\mathbf{U}}_i^n(x_{i+1/2}), \widetilde{\mathbf{U}}_{i+1}^n(x_{i+1/2})\right) - \boldsymbol{\mathcal{F}}\left(\widetilde{\mathbf{U}}_{i-1}^n(x_{i-1/2}), \widetilde{\mathbf{U}}_i^n(x_{i-1/2})\right)\right), \tag{2.4}$$

where $\widetilde{\mathbf{U}}_i^n(x_{i+1/2})$ is the polynomial reconstruction of the solution on cell i evaluated at $x_{i+1/2}$ defined by (2.3).

To get the same order in space and time a method of lines may be used. Good candidates for the time integrators are Total Variation Diminishing (TVD) [51, 52, 31] or Strong-Stability Preserving (SSP) [32, 53, 54, 50, 30, 49, 42] time schemes. Those schemes are very interesting as it is directly possible to use them in place of the forward Euler scheme and get a high-order scheme in time. This is possible since their CFL conditions are directly linked to the one of the forward Euler scheme [41].

For instance, in this work, the time schemes used for the numerical tests are: the forward Euler, SSPRK$(2,2)$, SSPRK$(3,3)$ and SSPRK$(5,4)$ schemes [53], where SSPRK(s,p) refers to an SSP RK scheme of order p with s stages. When using a time scheme with more stages than the order ($s > p$), the stability of the scheme is increased and the global computational time can decrease due to less re-computations. In this paper, we will only make reference to explicit discretization in time, as it is known [21, 44, 37, 30] that the high-order implicit SSP schemes are not computationally efficient for very high-order because their CFL condition become at most twice the one of the forward Euler method.

2.2. First-order scheme for the full system

Next, let us recall the HLL-AP scheme from [7] to get an approximated solution of the system with source term (1.1). We choose to work with the HLL-AP scheme as the construction of the 2D scheme is based on this scheme: the HLL-DLP-AP flux from [9] uses it in several directions. Hence, this part aims to introduce the various techniques without dealing with the difficulties of the 2D unstructured meshes.

This scheme is obtained by introducing the source term in the approximate Riemann solver and has the AP property. In its classical form the HLL-AP scheme can be written as:

$$\mathbf{U}_i^{n+1} = \mathbf{U}_i^n - \frac{\Delta t}{\Delta x}\left(\alpha_{i+1/2}\boldsymbol{\mathcal{F}}_{i+1/2} - \alpha_{i-1/2}\boldsymbol{\mathcal{F}}_{i-1/2}\right) + \frac{\Delta t}{\Delta x}\mathbf{S}_i^n. \tag{2.5}$$

This scheme is consistent with (1.1), stable and conserves the set of admissible states $\mathcal{A}$ under the same hyperbolic CFL condition as the scheme for the homogeneous system (2.1):

$$\frac{\Delta t}{\Delta x}\max_i\left(|b_{i+1/2}^-|, |b_{i+1/2}^+|\right) \leq \frac{1}{2}. \tag{2.2}$$

The α coefficients define a convex combination between the mean values and the discretization of the source term. Those coefficients are defined as:

$$\alpha(\mathbf{U}_i, \mathbf{U}_{i+1/2}) = \alpha_{i+1/2} = \frac{b_{i+1/2}^+ - b_{i+1/2}^-}{b_{i+1/2}^+ - b_{i+1/2}^- + (\gamma_{i+1/2} + \overline{\gamma}_{i+1/2})\Delta x}, \tag{2.6}$$

with $\gamma_{i+1/2} = \gamma\left(\frac{\mathbf{U}_i + \mathbf{U}_{i+1}}{2}\right)$ and $\overline{\gamma} > 0$ the AP correction. This correction is introduced to reach the right diffusive limit by applying the scheme on the following system, equivalent to (1.1):

$$\partial_t \mathbf{U} + \operatorname{div}(\mathbf{F}(\mathbf{U})) = (\gamma(\mathbf{U}) + \overline{\gamma})(\overline{\mathbf{R}}(\mathbf{U}) - \mathbf{U}), \tag{2.7}$$

which defines:

$$\overline{\mathbf{R}}(\mathbf{U}) := \frac{\gamma(\mathbf{U})\mathbf{R}(\mathbf{U}) + \overline{\gamma}\mathbf{U}}{\gamma(\mathbf{U}) + \overline{\gamma}}. \tag{2.8}$$

Then, the form of the free parameter $\overline{\gamma}$ is set in order to target a specific scheme in the diffusive limit. Finally, the source term is discretized using the following quantities:

$$\begin{aligned}
\mathbf{S}_i^n &= (1-\alpha_{i-1/2})\mathbf{S}_{i-1/2}^+ + (1-\alpha_{i+1/2})\mathbf{S}_{i+1/2}^-, \\
\mathbf{S}_{i+1/2}^- &= \min(0, b_{i+1/2}^-)\left(\mathbf{U}_i^n - \overline{\mathbf{R}}_{i+1/2}\right) \\
&\quad + \min(0, b_{i+1/2}^+)\left(\overline{\mathbf{R}}_{i+1/2} - \mathbf{U}_{i+1}^n\right) - \mathbf{F}(\mathbf{U}_i^n), \\
\mathbf{S}_{i-1/2}^+ &= \max(0, b_{i-1/2}^-)\left(\mathbf{U}_{i-1}^n - \overline{\mathbf{R}}_{i-1/2}\right) \\
&\quad + \max(0, b_{i-1/2}^+)\left(\overline{\mathbf{R}}_{i-1/2} - \mathbf{U}_i^n\right) + \mathbf{F}(\mathbf{U}_i^n),
\end{aligned}$$

$\overline{\mathbf{R}}_{i+1/2} = \dfrac{\gamma(\mathbf{U}_i^n)\mathbf{R}(\mathbf{U}_i^n) + \overline{\gamma}_{i+1/2}\mathbf{U}_i^n}{\gamma(\mathbf{U}_i^n) + \overline{\gamma}_{i+1/2}}$. Let us remark, that if the source term is not present ($\gamma = 0$), then HLL-AP scheme (2.5) is nothing but the classical finite volume schemes (2.1), as $\alpha_{i+1/2|\gamma=0} = 1$.

As an illustration, when $\gamma t \to \infty$ and with the right $\overline{\gamma}$, the limit of the scheme (2.5) for the isentropic Euler model with friction (1.4) is:

$$\rho_i^{n+1} = \rho_i^n + \frac{\Delta t}{\Delta x^2}\left(\frac{p'(\rho_{i+1/2}^n)}{\kappa_{i+1/2}^n}(\rho_{i+1}^n - \rho_i^n) - \frac{p'(\rho_{i-1/2}^n)}{\kappa_{i-1/2}^n}(\rho_i^n - \rho_{i-1}^n)\right), \tag{2.9}$$

which is consistent with the limit equation (1.5).

2.3. High-order scheme for the full system

The HLL-AP scheme from [7] recalled in (2.5) is consistent and stable, conserves the set of admissible states $\mathcal{A}$ under a classical hyperbolic CFL condition (2.2) and is AP. Moreover, it is only a first-order scheme. High-order schemes may be needed to correctly describe discontinuities that can appear in the transport regime, without the need of a very fine mesh.

There a two main difficulties that arise to extend the first-order HLL-AP to high-order. First, the choice of the α coefficients (2.6) from [7] forbids the scheme to be high-order in every regime. Indeed, this would require the following properties to hold:

$$\begin{cases}
\alpha_{i+1/2} \in [0;1] \\
\alpha_{i+1/2} = 1 + \mathcal{O}(\Delta x^2) \ \left(\text{or at least } \alpha_{i+1/2} - \alpha_{i-1/2} = \mathcal{O}(\Delta x^3)\right) \\
\dfrac{1-\alpha_{i-1/2}}{\Delta x}\mathbf{S}_{i-1/2}^+ + \dfrac{1-\alpha_{i+1/2}}{\Delta x}\mathbf{S}_{i+1/2}^- = \gamma(\mathbf{U}_i^n)(\mathbf{R}(\mathbf{U}_i^n) - \mathbf{U}_i^n) + \mathcal{O}(\Delta x^2)
\end{cases}. \tag{2.10}$$

The last two properties are mutually exclusive, hence the scheme with this choice of α cannot reach a uniform high-order. The second difficulty is that high-order extensions of parabolic schemes are more suited to polynomial reconstructions per interface instead of the cell reconstructions (2.3). Hopefully, the limit diffusion is slow compared to the hyperbolic time scales and therefore, the benefits of high-order are expected to mainly occur near the transport regime, where the limiting effects of the α coefficient on the order can be overcome.

Consequently, a new coefficient β is introduced to get a high-order scheme in the transport regime ($\gamma \sim 0$) and the first-order scheme in the diffusive limit ($\gamma t \gg 1$) to recover the AP

property. Hence, β_i^n is defined in order to create a convex combination between the polynomial reconstruction $\widetilde{\mathbf{U}}_i^n$ (2.3) and the mean value $\mathbf{U}_i^n$ on cell i at time t^n:

$$\overline{\mathbf{U}}_i^n(x) := \beta_i^n \widetilde{\mathbf{U}}_i^n(x) + (1-\beta_i^n)\mathbf{U}_i^n, \tag{2.11}$$

where β_i^n needs to fulfil the following properties:

$$\begin{cases} \beta_i^n & \in [0;1] \\ \beta_i^n & \xrightarrow[\gamma t\to\infty]{} 0 \\ \beta_i^n & \xrightarrow[\gamma\to 0]{} 1 \\ \beta_i^n & = 1+\mathcal{O}(\Delta x) \end{cases}. \tag{2.12}$$

The first property allows to properly define the convex combination and the two others permit to have the limit scheme in the diffusive limit and the high-order scheme in the transport regime. The last property ensures that the scheme with the high-order polynomial reconstruction is used on fine meshes as the scheme is able to properly discretize the source term. One possible choice, among all the possibilities that satisfy the properties (2.12) is:

$$\beta_i^n := \frac{\Delta_l}{\Delta_l + \gamma_i^n t^n \Delta x}, \tag{2.13}$$

where $\gamma_i = \gamma(\mathbf{U}_i^n)$ and Δ_l is a characteristic length. This characteristic length has to be chosen such that the high-order polynomial reconstruction $\widetilde{\mathbf{U}}_i^n$ takes the leads in the transport regime ($\gamma t \Delta x \simeq 1$), whereas, the mean values dominates in the diffusive limit ($\gamma t \Delta x \gg 1$). The numerical tests show that $\Delta_l := 5\times 10^{-2} L$ is a reasonable choice, where L is a characteristic length of the computational domain. The effects of a change of Δ_l can be observed by comparing the numerical results in 1D (Tables 1, 2 and 3) and 2D (Tables 6, 7 and 8) as there is a multiplicative factor between the two space steps. Let us remark that this change only modify the transitional area between the use of the mean values and polynomial reconstruction. In fact, with the properties (2.12) the scheme is always AP when $\gamma t \to \infty$.

In addition to provide a simple extension of the first-order scheme (2.5) this convex combination allows to only use one polynomial reconstruction by cell.

Next, to get the high-order HLL-AP scheme, one has to use the values of the new convex combination $\overline{\mathbf{U}}(x)$ evaluated on the interfaces in the scheme (2.5) and use an appropriate time scheme. For instance, with a forward Euler discretization in time, the scheme is:

$$\begin{aligned} \mathbf{U}_i^{n+1} =& \mathbf{U}_i^n - \frac{\Delta t}{\Delta x}\Big(\alpha\left(\overline{\mathbf{U}}_i^n(x_{i+1/2}), \overline{\mathbf{U}}_{i+1}^n(x_{i+1/2})\right)\boldsymbol{\mathcal{F}}\left(\overline{\mathbf{U}}_i^n(x_{i+1/2}), \overline{\mathbf{U}}_{i+1}^n(x_{i+1/2})\right) \\ & - \alpha\left(\overline{\mathbf{U}}_{i-1}^n(x_{i-1/2}), \overline{\mathbf{U}}_i^n(x_{i-1/2})\right)\boldsymbol{\mathcal{F}}\left(\overline{\mathbf{U}}_{i-1}^n(x_{i-1/2}), \overline{\mathbf{U}}_i^n(x_{i-1/2})\right)\Big) \\ & + \frac{\Delta t}{\Delta x}\mathbf{S}_i^n(\overline{\mathbf{U}}). \end{aligned} \tag{2.14}$$

Finally, to prove the AP property we need to investigate the asymptotic behaviour of the high-order scheme (2.14) when $\gamma t \to \infty$. Rigorous techniques based on [8] may be considered, however we will only use a classical Champmann-Enskog expansion here since it provides the correct limit.

Hence, $\varepsilon > 0$ is introduced to make the following rescaling:

$$\begin{cases} \gamma & \leftarrow \dfrac{\gamma}{\varepsilon} \\ \Delta t & \leftarrow \dfrac{\Delta t}{\varepsilon} \end{cases} \tag{2.15}$$

In order to get the limit one can assume that the wave speeds and γ are continuous and let us notice, that according to (2.12):

$$\overline{\mathbf{U}}_i^n(x) = \beta_i^n \widetilde{\mathbf{U}}_i^n(x) + (1-\beta_i^n)\mathbf{U}_i^n \xrightarrow[\gamma t \to \infty]{} \mathbf{U}_i^n.$$

The previous rescaling (2.15) induced the following expansions:

$$\begin{cases} \Delta t\ \alpha_{i+1/2} &= \Delta t \dfrac{b_{i+1/2}^+ - b_{i+1/2}^-}{(b_{i+1/2}^+ - b_{i+1/2}^-)\varepsilon + (\gamma_{i+1/2} + \overline{\gamma}_{i+1/2})\Delta x} \\ &= \Delta t \dfrac{b_{i+1/2}^+ - b_{i+1/2}^-}{(\gamma_{i+1/2} + \overline{\gamma}_{i+1/2})\Delta x} + \mathcal{O}(\varepsilon) \\ \Delta t\ (1-\alpha_{i+1/2}) &= \Delta t \dfrac{(\gamma_{i+1/2} + \overline{\gamma}_{i+1/2})\Delta x}{(b_{i+1/2}^+ - b_{i+1/2}^-)\varepsilon^2 + (\gamma_{i+1/2} + \overline{\gamma}_{i+1/2})\Delta x \varepsilon} \\ &= \dfrac{\Delta t}{\varepsilon} - \Delta t \dfrac{b_{i+1/2}^+ - b_{i+1/2}^-}{(\gamma_{i+1/2} + \overline{\gamma}_{i+1/2})\Delta x} + \mathcal{O}(\varepsilon) \\ \beta_i^n &= \dfrac{\varepsilon^2 \Delta_l}{\varepsilon^2 \Delta_l + (\gamma_i + \overline{\gamma}_i) t^n \Delta x} = \mathcal{O}(\varepsilon^2) \end{cases} . \tag{2.16}$$

By introducing the expansions (2.16) in the scheme (2.14), and identifying the powers of ε, it leads first for the ε^{-1} terms:

$$0 = \frac{\Delta t}{\Delta x}\left(\mathbf{S}_{i-1/2}^+(\mathbf{U}) + \mathbf{S}_{i+1/2}^-(\mathbf{U})\right),$$

which implies $\mathbf{R}(\mathbf{U}) = \mathbf{U}$. Then, for the ε^0 terms:

$$\begin{aligned} \mathbf{U}_i^{n+1} = \mathbf{U}_i^n &- \frac{\Delta t}{\Delta x^2}\left(\frac{b_{i+1/2}^+ - b_{i+1/2}^-}{\gamma_{i+1/2} + \overline{\gamma}_{i+1/2}} \boldsymbol{\mathcal{F}}(\mathbf{U}_{i+1}^n, \mathbf{U}_i^n) - \frac{b_{i-1/2}^+ - b_{i-1/2}^-}{\gamma_{i-1/2} + \overline{\gamma}_{i-1/2}} \boldsymbol{\mathcal{F}}(\mathbf{U}_i^n, \mathbf{U}_{i-1}^n)\right)_{|\overline{\mathbf{R}}(\mathbf{U})=\mathbf{U}} \\ &- \frac{\Delta t}{\Delta x^2}\left(\frac{b_{i+1/2}^+ - b_{i+1/2}^-}{\gamma_{i+1/2} + \overline{\gamma}_{i+1/2}} \mathbf{S}_{i+1/2}(\mathbf{U}_{i+1}^n, \mathbf{U}_i^n) + \frac{b_{i-1/2}^+ - b_{i-1/2}^-}{\gamma_{i-1/2} + \overline{\gamma}_{i-1/2}} \mathbf{S}_{i-1/2}(\mathbf{U}_i^n, \mathbf{U}_{i-1}^n)\right)_{|\overline{\mathbf{R}}(\mathbf{U})=\mathbf{U}} . \end{aligned} \tag{2.17}$$

Let us notice that the expression for the ε^0 terms (2.17) is independent of the high-order polynomial reconstruction thanks to the definition of $\overline{\mathbf{U}}_i^n$ (2.11). Thus, the asymptotic preserving correction $\overline{\gamma}$ for the high-order HLL-AP scheme (2.14) is the same as for the first-order HLL-AP scheme (2.5) from [7].

Finally, the high-order version of the HLL-AP scheme (2.14) is a high-order scheme in the transport regime and degenerates to the same limit scheme as the first-order HLL-AP scheme (2.5).

3. 1D numerical results

3.1. 1D Riemann problems with the Telegraph equations

In order to inspect the behaviour of the high-order HLL-AP scheme (2.14) developed in the previous section, we first compare the results between the new scheme and reference solutions for the Telegraph [40, 29] equations (or Goldstein-Taylor [28, 55]) in 1D:

$$\left\{ \begin{array}{rcl} \partial_t u + a\partial_x u &=& \sigma(v-u) \\ \partial_t v - a\partial_x v &=& \sigma(u-v) \end{array} \right. , \tag{3.1}$$

with $a > 0$ and $\sigma > 0$. Those equations enter in the framework of (1.1) with:

$$\mathbf{U} = \begin{pmatrix} u \\ v \end{pmatrix}, \ \mathbf{F}(\mathbf{U}) = \begin{pmatrix} au \\ -av \end{pmatrix}, \ \mathbf{R}(\mathbf{U}) = \begin{pmatrix} v \\ u \end{pmatrix}, \tag{3.2}$$

where $\gamma(\mathbf{U}) = \sigma > 0$. When $\sigma t \to \infty$, the system (3.1) degenerates into the following limit equation on $(u+v)$, on the local map of the equilibrium $u - v = 0$ ($\mathbf{R}(\mathbf{U}) = \mathbf{U}$):

$$\partial_t(u+v) - \partial_x \left(\frac{a^2}{2\sigma} \partial_x (u+v) \right) = 0. \tag{3.3}$$

Those reference solutions for Riemann problems are constructed in Appendix A using two methods. The first one (M1) uses a reformulation of the system (3.1) and a finite difference scheme. The second one (M2) is set up with a power series decomposition of the solution.

3.1.1. Comparison between the two methods

First, the two methods to obtain the reference solutions are compared on the following test case: $\sigma = 1$, $a = 0.5$ with a final time $t = 1$. The initial left state is defined as $\mathbf{U}_L = (-1 \ 0)^T$ and $\mathbf{U}_R = (1 \ -1)^T$ for the right initial state. This test is constructed in order that the two methods are well defined and to present a solution with different behaviours.

The solution is plotted in Figure 3, with $\Delta x = 2 \cdot 10^{-3}$ for the space discretization. The substitution method (M1) uses 1000 points and in the power series method (M2) 10 ODEs from (A.9) are solved numerically. As it could be seen in Figure 3 the two methods give the same result with a complex structure in the central zone. Let us remark that due to the presence of the source term, the left and right states are not constant in time (see (A.3) and (A.4)) as with a usual Riemann problem for a homogeneous hyperbolic system (1.2).

3.1.2. Comparison with a continuous σ

Using the same initialisation as for the comparison between the two methods we make a comparison with the HLL-AP scheme in Figure 4. The results are presented with 80 cells, and the high-order scheme uses a polynomial reconstruction of degree 1 ($\mathbb{P}_1$). The curves in Figure 4 show that the high-order version of the scheme gives a better description of the discontinuities, and the spurious oscillations can be easily cut with the DMP limiter of the MOOD method.

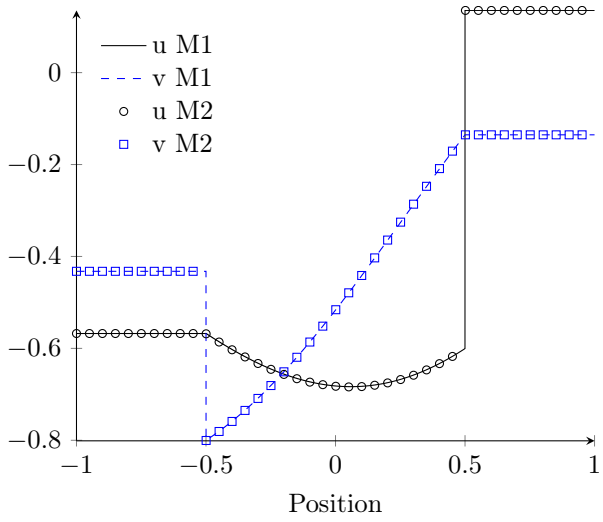

Figure 3: Comparison between the substitution method (M1) and the power series method (M2)

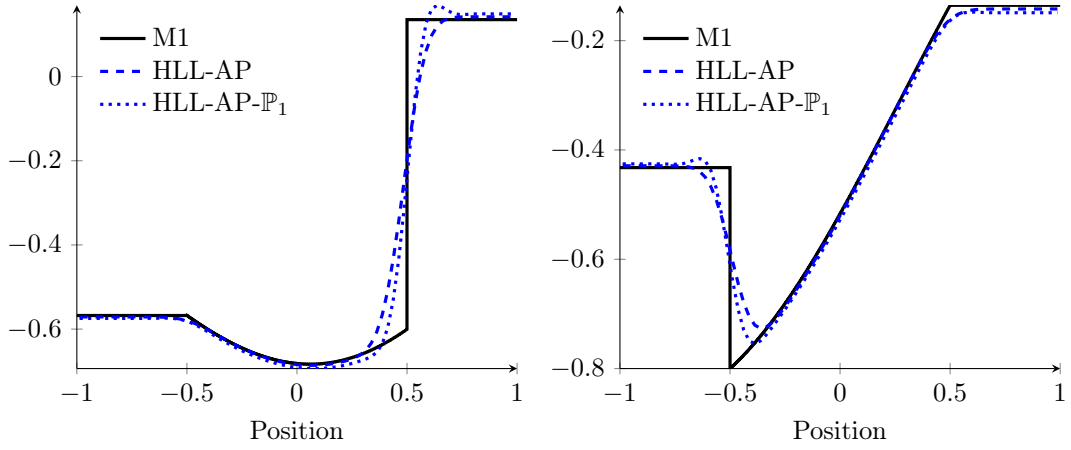

Figure 4: Comparison between the results obtained by M1, HLL-AP and HLL-AP-$\mathbb{P}_1$ with $\Delta x = 2.5 \cdot 10^{-2}$: u on the left and v on the right

3.1.3. Comparison with a discontinuous σ

The next case use the same initialisation as the previous one with a discontinuous σ:

$$\sigma(x) = \begin{cases} \sigma_L = 0.1 & \text{if } x < 0 \\ \sigma_R = 1.0 & \text{otherwise.} \end{cases}$$

Here, only the power series method (M2) can be used. The results are also compared to the HLL-AP and the HLL-AP-$\mathbb{P}_1$ schemes on 80 cells in Figure 5. This figure shows that both schemes capture the discontinuity of σ. Besides, as previously the high-order scheme gives a better description of the discontinuities.

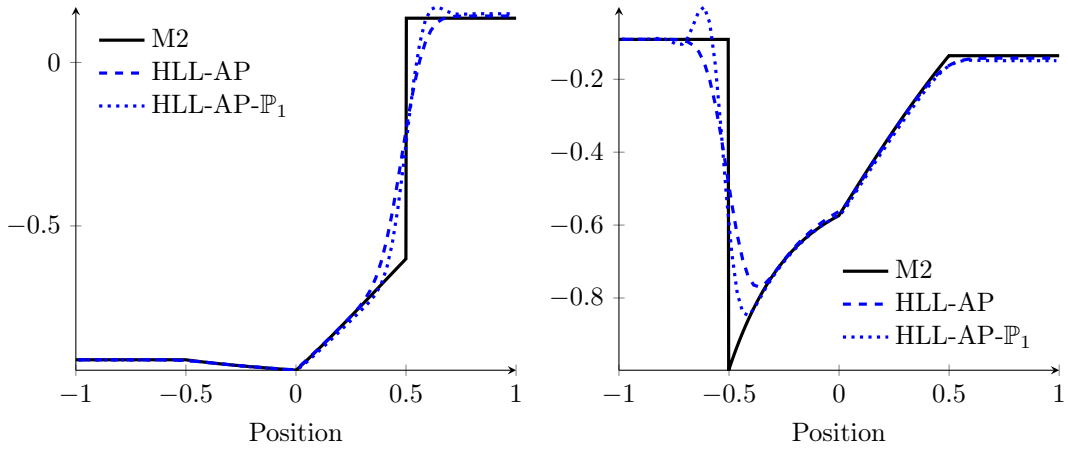

Figure 5: Comparison between the results obtained by M2, HLL-AP and HLL-AP-$\mathbb{P}_1$ with $\Delta x = 2.5 \cdot 10^{-2}$: u on the left and v on the right

3.1.4. Comparison with a discontinuous σ and the DMP

In order to show that the oscillations can be easily cleaned, a result with the same initialisation with a discontinuous σ and 80 cells is presented in Figure 6. The second-order HLL-AP scheme (HLL-AP-$\mathbb{P}_1$) without limitations and the same scheme limited with the DMP (HLL-AP-$\mathbb{P}_1$-DMP) on u and v are compared to the reference solution obtained by the power series method (M2). In the zoom of Figure 6, one can see that the spurious oscillation near the discontinuity is deleted with the DMP limiter and the precision is improved compared to the HLL-AP-$\mathbb{P}_0$ scheme.

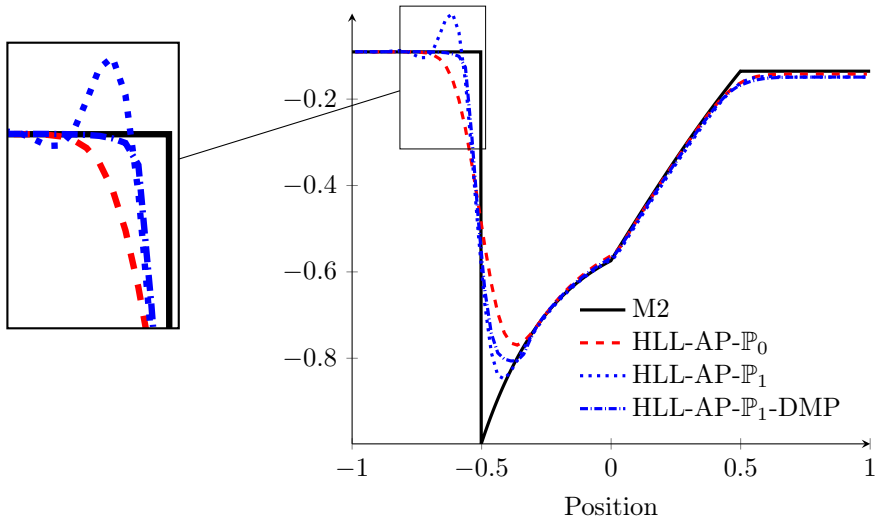

Figure 6: Comparison between on v of the results obtained by M2, HLL-AP-$\mathbb{P}_0$, HLL-AP-$\mathbb{P}_1$, and HLL-AP-$\mathbb{P}_1$ limited with the DMP on a mesh of size $\Delta x = 2.5 \cdot 10^{-2}$

3.2. Smooth solutions and order

After the comparison and the study of the behaviour of the high-order scheme regarding to some discontinuous solutions, the next test cases are set up with some smooth solutions. This second comparison is made in order to tackle with the real order of the high-order version of the HLL-AP scheme (2.14). The solutions computed by the schemes are compared to a set of smooth exact solutions obtained with the same method used for the hyperbolic heat equation in [14, 16]. The reader is referred to Appendix B for more details about the construction of those solutions.

In Tables 1, 2 and 3 the comparison is made between the first-order scheme and the high-order version using the convex combination with the β coefficients. In those tables the errors are the relative errors computed in L^2-norm on u (the results on v are similar) regarding to the exact solution described in Appendix B. The results are obtained on uniform meshes of $[0; 1]$ with $a = 1$. Dirichlet boundary conditions are used with the exact solution on both sides. All the quantities are computed at the final time $t = 1$.

Mesh		β	$\mathbb{P}_0$		$\mathbb{P}_1$		$\mathbb{P}_2$		$\mathbb{P}_3$	
Nb. cells	Δx	(2.13)	e_{L^1}	p_{L^2}	e_{L^2}	p_{L^2}	e_{L^2}	p_{L^2}	e_{L^2}	p_{L^2}
160	6.25E-03	1.00	3.60E-02	—	8.14E-04	—	6.99E-05	—	5.29E-05	—
320	3.13E-03	1.00	1.82E-02	0.98	2.07E-04	1.98	1.53E-05	2.19	1.32E-05	2.01
640	1.56E-03	1.00	9.18E-03	0.99	5.21E-05	1.99	3.54E-06	2.12	3.26E-06	2.01
1 280	7.81E-04	1.00	4.60E-03	1.00	1.31E-05	1.99	8.35E-07	2.08	8.01E-07	2.03
2 560	3.91E-04	1.00	2.30E-03	1.00	3.27E-06	2.00	1.97E-07	2.09	1.92E-07	2.06
5 120	1.95E-04	1.00	1.15E-03	1.00	8.17E-07	2.00	4.49E-08	2.13	4.43E-08	2.12
10 240	9.77E-05	1.00	5.76E-04	1.00	2.03E-07	2.01	9.36E-09	2.26	9.28E-09	2.26

Table 1: Convergence rates with $\sigma = 10^{-2}$ and $t = 1$

In Table 1 the source term is not preponderant and the high-order scheme is clearly better than the first-order scheme. The precision is increased as the scheme uses mainly the polynomial reconstruction $\widetilde{\mathbf{U}}$ in the convex combination created with β (2.11). More in details, the reconstruction of degree 1 reaches the second-order, whereas, the third-order is not reached with the $\mathbb{P}_2$ reconstruction even if the precision is still improved. Then, a limit is reached when using a polynomial reconstruction of degree greater than 2, where the impact of the reconstruction is not visible in this configuration.

Mesh		β	$\mathbb{P}_0$		$\mathbb{P}_1$		$\mathbb{P}_2$		$\mathbb{P}_3$	
Nb. cells	Δx	(2.13)	e_{L^1}	p_{L^2}	e_{L^2}	p_{L^2}	e_{L^2}	p_{L^2}	e_{L^2}	p_{L^2}
160	6.25E-03	0.89	3.89E-02	—	3.18E-03	—	3.19E-03	—	3.17E-03	—
320	3.13E-03	0.94	1.97E-02	0.98	5.31E-04	2.58	6.51E-04	2.29	6.50E-04	2.29
640	1.56E-03	0.97	9.88E-03	0.99	3.37E-04	0.66	3.75E-04	0.80	3.75E-04	0.79
1 280	7.81E-04	0.98	4.95E-03	1.00	2.39E-04	0.49	2.47E-04	0.60	2.47E-04	0.60
2 560	3.91E-04	0.99	2.48E-03	1.00	1.40E-04	0.78	1.42E-04	0.81	1.42E-04	0.81
5 120	1.95E-04	1.00	1.24E-03	1.00	7.50E-05	0.90	7.55E-05	0.91	7.55E-05	0.91
10 240	9.77E-05	1.00	6.20E-04	1.00	3.88E-05	0.95	3.89E-05	0.95	3.89E-05	0.95

Table 2: Convergence rates with $\sigma = 1$ and $t = 1$

With a larger source term in Table 2 the high-order scheme is again more accurate than the first-order scheme even if the second-order is not reached as expected. This can be explained with a previous remark regarding to the properties (2.10) that the α coefficients developed in [7] need to fulfill in order to have a second-order scheme with source term. Here, the limitation can be seen since the $\mathbb{P}_2$ reconstruction is not more precise than the $\mathbb{P}_1$.

Mesh		β	$\mathbb{P}_0$		$\mathbb{P}_1$		$\mathbb{P}_2$		$\mathbb{P}_3$	
Nb. cells	Δx	(2.13)	e_{L^1}	p_{L^2}	e_{L^2}	p_{L^2}	e_{L^2}	p_{L^2}	e_{L^2}	p_{L^2}
160	6.25E-03	0.44	1.01E-02	—	1.11E-01	—	1.11E-01	—	1.11E-01	—
320	3.13E-03	0.62	4.93E-03	1.03	6.49E-02	0.75	6.49E-02	0.78	6.49E-02	0.78
640	1.56E-03	0.76	2.44E-03	1.01	3.57E-02	0.84	3.57E-02	0.86	3.57E-02	0.86
1 280	7.81E-04	0.86	1.21E-03	1.01	1.88E-02	0.91	1.88E-02	0.92	1.88E-02	0.92
2 560	3.91E-04	0.93	6.06E-04	1.00	9.69E-03	0.95	9.69E-03	0.96	9.69E-03	0.96
5 120	1.95E-04	0.96	3.02E-04	1.00	4.92E-03	0.98	4.92E-03	0.98	4.92E-03	0.98
10 240	9.77E-05	0.98	1.51E-04	1.00	2.48E-03	0.99	2.48E-03	0.99	2.48E-03	0.99

Table 3: Convergence rates with $\sigma = 10$ and $t = 1$

Finally, in the intermediary regime with an even larger source term in Table 3, the convergence is slower for the high-order than the first-order as there is a competition between the two schemes in addition of the convex combination between the numerical flux and the source term with the α coefficients from (2.6).

Let us emphasize, that for all these computations no limiter is used in the MOOD loop. The order is only limited as the computations are done with the convex combination created by the β coefficients (2.13) in $\overline{\mathbf{U}}$ (2.11).

With those three tables we can see the behaviour of the high-order HLL-AP scheme regarding to smooth solutions. The $\mathbb{P}_1$ reconstruction significantly improves the results except very close to the diffusion limit, whereas the $\mathbb{P}_2$ and $\mathbb{P}_3$ are less useful in this case mainly due to the limitations of the α coefficients and the regularity of the solutions. This conclusion needs to be linked with more meaningful results in more complex situations in 2D (see Figures 15 and 16) where the polynomial reconstruction gives better results. Moreover, those results are strongly linked to the choice of the β coefficient which determines when the high-order polynomial reconstruction is used.

Remark 3.1. *The tests are not run for $\sigma \gg 10$ as the exact solutions involve the computations of some exponential functions which are not well defined numerically in those scales. Besides, no tests are made with $\sigma = 0$ in this section as the behaviour of the high-order homogeneous scheme (2.4) is well-known. For the 2D case without source term, one may see the results in Table 5.*

3.3. Convergence to the diffusion with late time

We now investigates with AP property of the scheme by looking at its convergence towards the diffusive regime. One way to reach the diffusion limit is to set κ and then to increase the final time. In order to do that the initial condition is a Gaussian in density:

$$\rho_0(x) = \exp(-(x-75)^2) + 1$$

with a null speed: $u_0(x) = 0$, so that the initial condition is well-prepared. The computational domain $[0; 150]$ is meshed with 3000 cells and Neumann boundary conditions are used on both

sides. This domain is chosen such that the solution does not approach the boundary, in order to avoid spurious effects. The final time of the simulation is $t = 100$ and during the simulations the L^2 and L^∞-norms of the density and the momentum are computed. For the density one has to remove the value of the equilibrium $\rho_E := 1$ in order to make the comparison easier. Then, according to [8] the variables satisfy:

$$\|\partial_x^\beta(\rho - \rho_E)\|_{L^p} = \mathcal{O}(1+\gamma t)^{-1/2(1-1/p)-\beta/2}$$
$$\|\partial_x^\beta(\rho u)\|_{L^p} = \mathcal{O}(1+\gamma t)^{-1/2(1-1/p)-\beta/2-1/2}$$

Besides, after some computations the time derivatives should verify :

$$\|\partial_t \rho\|_{L^p} = \mathcal{O}(1+\gamma t)^{-1/2(1-1/p)-1}$$
$$\|\partial_t(\rho u)\|_{L^p} = \mathcal{O}(1+\gamma t)^{-1/2(1-1/p)-3/2}$$

In Figures 7 to 9 and C.20 to C.22 (in appendix) the L^2 and L^∞-norms for the HLL-AP and the HLL-AP-$\mathbb{P}_1$ are plotted over time for $\kappa = 1$ and $\kappa = 5$. For each figure, we present the results and the theoretical slopes.

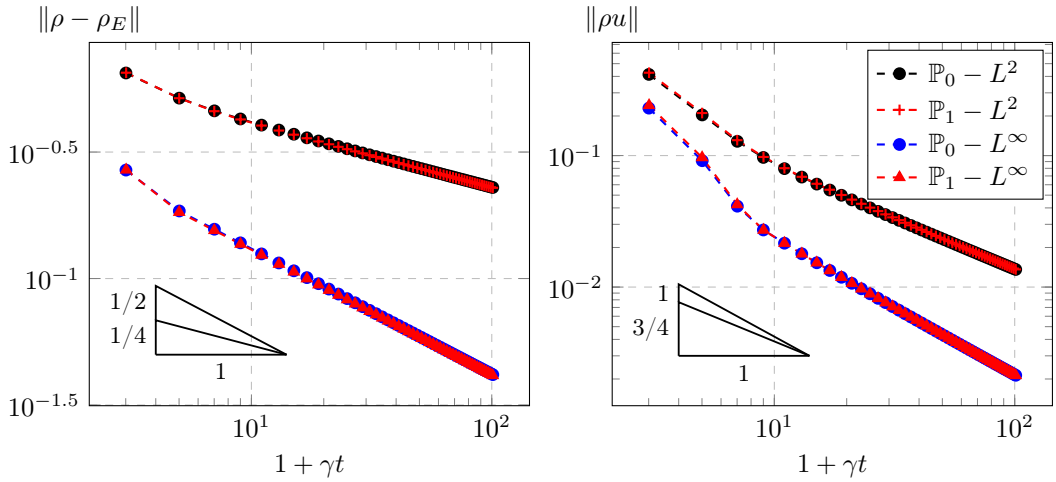

Figure 7: Convergence speeds to the equilibrium in L^2 and L^∞-norms for density and momentum with $\Delta x = 5\times10^{-2}$ and $\kappa = 1$ in 1D

The space and time derivatives are computed using classical centered and upwind finite differences approximations :

$$\partial_x f_i^{n+1} \simeq \frac{f_{i+1}^{n+1} - f_{i-1}^{n+1}}{2\Delta x}$$
$$\partial_x^2 f_i^{n+1} \simeq \frac{f_{i+1}^{n+1} - 2f_i^{n+1} + f_{i-1}^{n+1}}{\Delta x^2}$$
$$\partial_t f_i^{n+1} \simeq \frac{f_i^{n+1} - f_{i-1}^{n}}{\Delta t^n}$$
$$\partial_t^2 f_i^{n+1} \simeq 2\frac{\Delta t^{n-1} f_i^{n+1} - (\Delta t^n + \Delta t^{n+1}) f_i^n + \Delta t^n f_i^{n-1}}{\Delta t^n(\Delta t^n + \Delta t^{n-1})^2 - (\Delta t^n + \Delta t^{n-1})\Delta t^{n2}}$$

where f_i^{n+1} is the mean value of the quantity on cell i at time $t^{n+1} = t^n + \Delta t^n$.

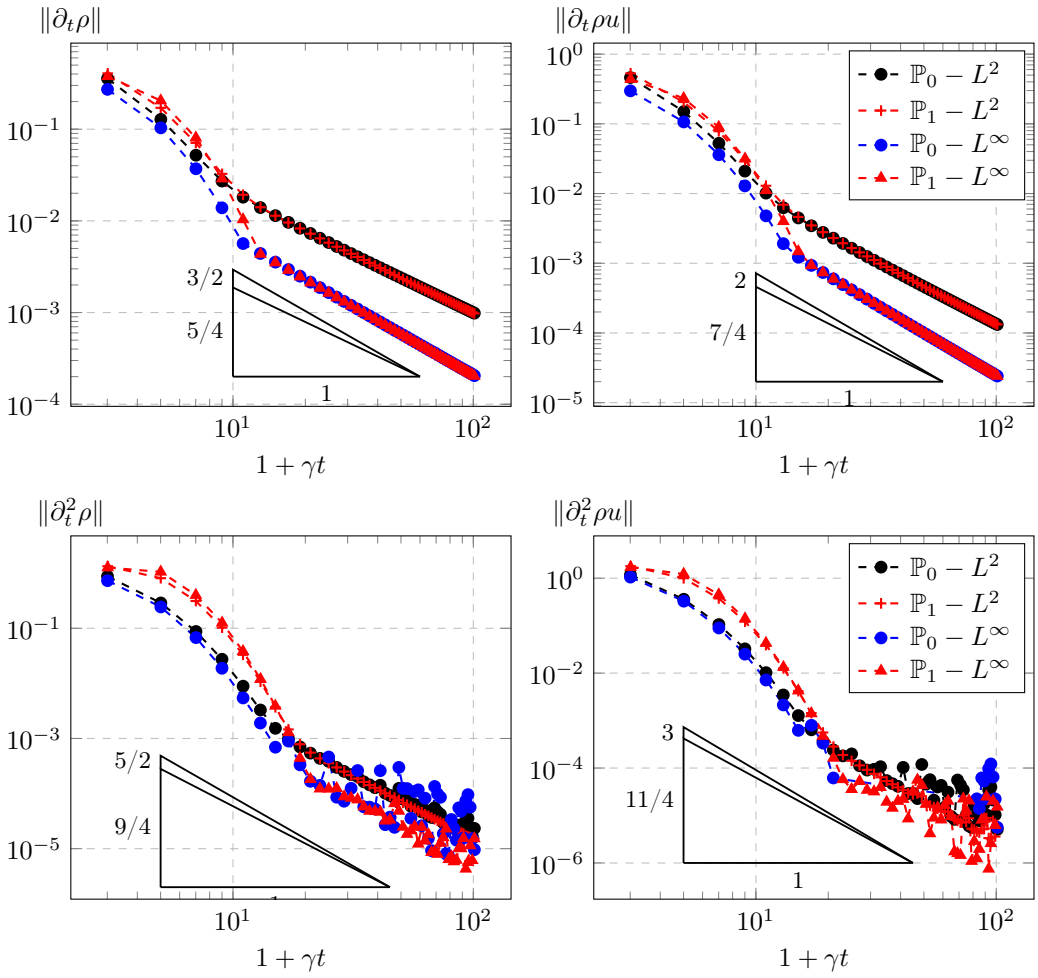

Figure 8: Convergence speeds to the equilibrium in L^2 and L^∞-norms for the time derivatives of the density and momentum with $\Delta x = 5 \times 10^{-2}$ and $\kappa = 1$ in 1D

We can see that for both values of the friction coefficient κ the first-order and the high-order scheme respect the convergence speeds to the equilibrium. For the high-order scheme as small transition is needed due to the β coefficient, however, the introduction of this new coefficient allows to preserve the right convergence speeds in all cases tested. If the coefficient β is too small, the high-order polynomial reconstruction will not be used and in the other hand if β is too large the transition area is longer. Only the second time derivatives in Figures 8 and C.21 are problematic with the presence of oscillations due to the numerical derivatives.

Indeed, if the scheme respects the various convergence rates for ρu, $\partial_x \rho$, $\partial_t \rho$, $\partial_x \rho u$ and $\partial_x^2 \rho$ it can be proved that the scheme will be AP, which is our case.

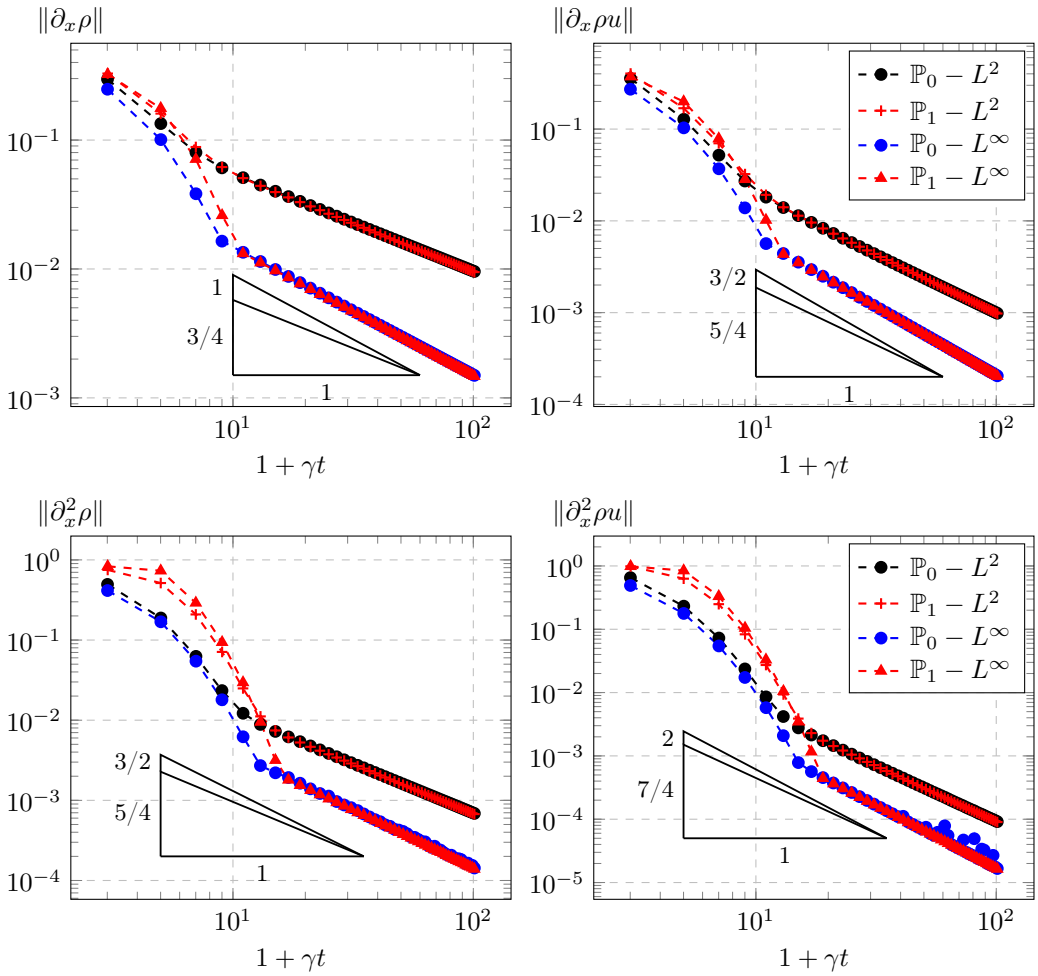

Figure 9: Convergence speeds to the equilibrium in L^2 and L^∞-norms for the space derivatives of the density and momentum with $\Delta x = 5 \times 10^{-2}$ and $\kappa = 1$ in 1D

One last check is made by comparing the solution obtained by the hyperbolic scheme and a parabolic one, on the limit equation near the diffusive regime. As with the previous figures, the diffusive limit is reached by setting κ and increasing the final time, contrary to the next test done in Table 4 and Figure 11 where the product γt is increasing.

Hence, in Figure 10 we compare the rates of convergence to the theory of [8]. Hence, the L^p-norm, with $p > 1$, of the difference should satisfy:

$$\|\partial_x^\beta(\rho_P - \rho_H)\|_{L^p} = \mathcal{O}(1+\gamma t)^{-1/2(1-1/p)-\beta/2-1/2} \tag{3.4}$$

As in Figure 11, the results are no so good than the previous comparison. This difference may be explained by the fact that ρ_P is not an analytical solution of (1.5) and rounding errors may disturb the convergence rates. With this last check, we can make a link with Table 3 to justify the fact

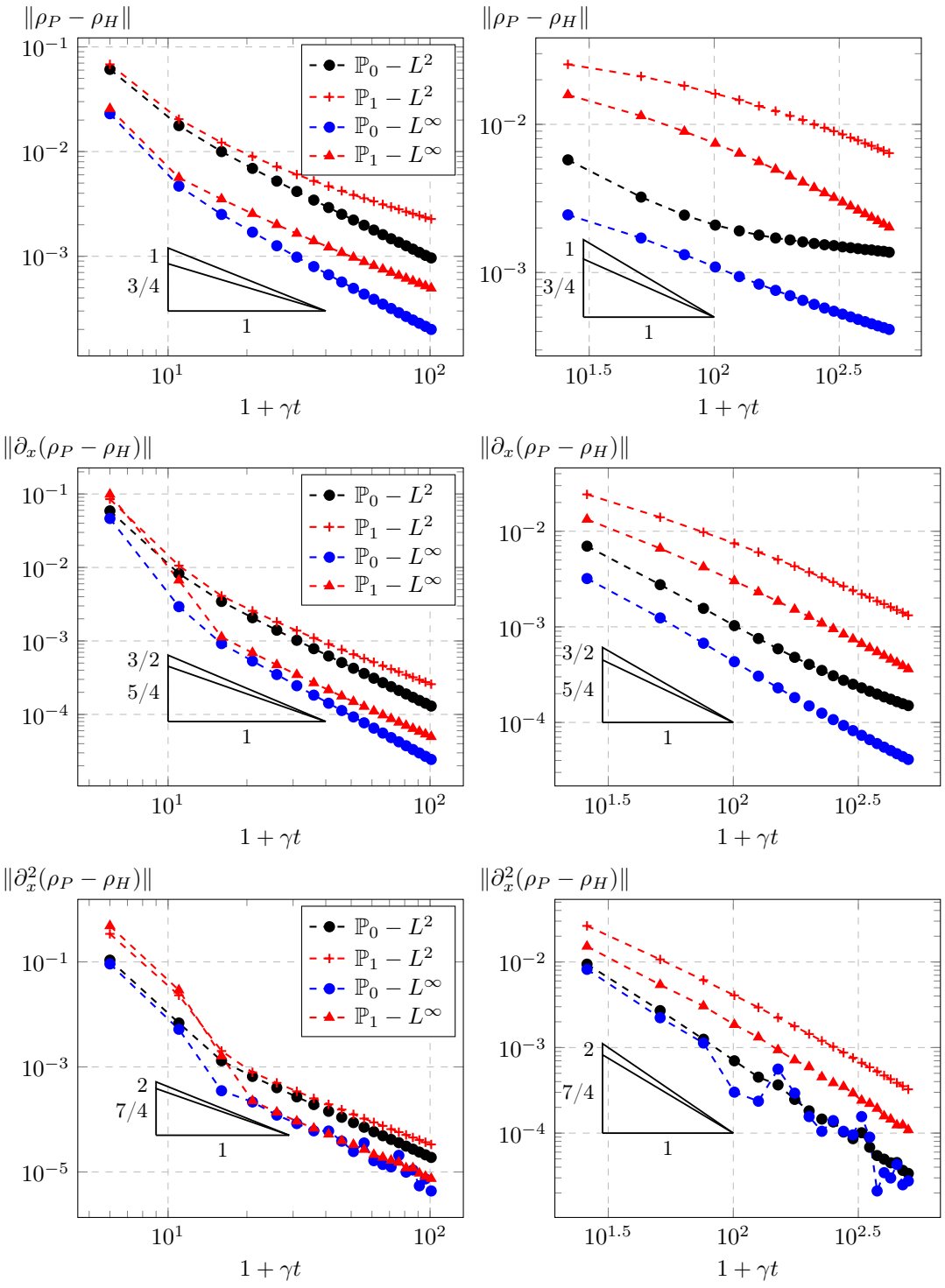

Figure 10: Convergence speeds to the diffusion limit with $\kappa = 1$ (left) and $\kappa = 5$ (right) compared to the theoretical rates (3.4) for the solution and its space derivatives

that the scheme with the $\mathbb{P}_1$ reconstruction converges slower than the first-order one to the diffusive limit. However, the overall behaviour is still satisfactory.

3.4. Convergence to the diffusion with increasing κt

The next test case also inspects the convergence to the diffusive limit. To do so, the isentropic Euler model with friction described by (1.4) is also used but, with an increasing γt. The domain is the segment $[0; 1]$ with a uniform mesh composed of 100 cells and Neumann boundary conditions are imposed. The solution given by the first-order and the second order HLL-AP schemes (ρ_H) are compared to the solution computed by a parabolic scheme (2.9) (ρ_P) on the limit equation (1.5). Besides, the comparison is also made with a non-AP scheme using a centered discretization of the source term:

$$\mathbf{U}_i^{n+1} = \mathbf{U}_i^n - \frac{\Delta t}{\Delta x}\left(\boldsymbol{\mathcal{F}}_{i+1/2} - \boldsymbol{\mathcal{F}}_{i-1/2}\right) + \Delta t \gamma(\mathbf{U}_i^n)\left(\mathbf{R}(\mathbf{U}_i^n) - \mathbf{U}_i^n\right). \tag{3.5}$$

Finally, the initialisation uses a Gaussian in density:

$$\rho_0(x) = \frac{1}{10}\left(\exp\left(-\frac{(x-1/2)^2}{2\cdot 0.05^2}\right) + 1\right),$$

with an initial speed set to zero: $u_0(x) = 0$, in order to be on the equilibrium map.

κ	1	5	25	125	625	3125
t	0.1	0.2	0.4	0.8	1.6	3.2
$\gamma t = \kappa t$	10^{-1}	1	10^1	10^2	10^3	10^4
β (2.13)	9.80E-01	8.33E-01	3.33E-01	4.76E-02	4.98E-03	5.00E-04
Scheme	$\|\rho_P - \rho_H\|_{L^2}$					
HLL-AP (2.5)	1.55E-02	6.97E-03	4.55E-04	1.08E-04	7.08E-05	3.38E-05
HLL-AP-$\mathbb{P}_1$ (2.14)	1.60E-02	7.97E-03	8.34E-04	4.95E-04	1.74E-04	2.85E-05
HLL-SRC (3.5)	1.54E-02	1.07E-02	2.16E-02	1.90E-02	2.08E-02	2.29E-02

Table 4: Convergence to the diffusion equation regarding to γt

In Table 4, it can be seen that both the first and second-order schemes converge to the diffusion limit, thanks to the definition of β (2.13). Whereas, the solution obtained by the scheme (3.5) does not converge to the diffusion solution when γt increases. The same results can be observed in Figure 11 with the theoretical rates (3.4) from [8].

The convergence speeds is not clearly reached as the solution of the diffusion equation ρ_P is computed numerically. Moreover, as $\kappa t \Delta x \simeq 1$ for most of the tests, we are in a intermediary regime where the asymptotic convergence speeds may not be reached yet.

Throughout those different tests, the behaviour of the scheme has been investigated. Let us underline that the HLL-AP scheme (2.5) and its high-order extension (2.14) are able to capture the solution in all the configurations tested: Riemann problems with reference solutions and smooth exact solutions. The high-order scheme is still AP thanks to the β coefficients (2.13) and the high-order polynomial reconstruction allows us to have a better description of the discontinuities in the transport regime.

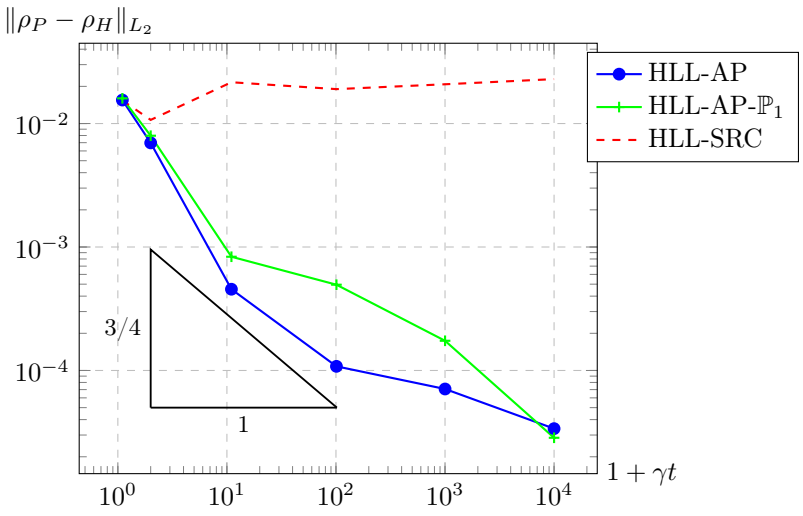

Figure 11: Convergence to the diffusion equation regarding to γt

4. Asymptotic and admissibility preserving scheme in 2D

After the presentation of the first-order scheme and the construction of the high-order scheme in 1D for both the homogeneous (1.2) and the full (1.1) systems, the next part of this work is devoted to the recall of the HLL-DLP and HLL-DLP-AP schemes in 2D from [9]. Those schemes are constructed using a reconstruction of fluxes that leads to schemes which have a proper numerical diffusion. This point is essential to get a consistent scheme in the diffusive limit with unstructured meshes. Then, using the same technique as in 1D, we construct the high-order version of those two schemes as they are based on a combination of the 1D schemes.

Hence, the outline of this part is similar to the one for 1D schemes. First, we recall some results for discretization of hyperbolic systems in 2D. Then, an extension to high-order is made. After that, the same methodology is applied to the HLL-DLP-AP scheme for the system with source term (1.1) where the use of a β coefficient is needed to preserve the AP property with the polynomial reconstruction of the MOOD method.

To describe a 2D unstructured mesh $\mathcal{M}$ composed of polygonal cells K the following notations are used:

- $|K|$: area of cell K,
- $\mathcal{E}_K$: set of interfaces of K,
- $|e_i|$: length of the i-th interface of K,
- $\mathbf{n}_{K,i}$: normal to interface i outgoing of cell K,
- L: neighbour of K by the edge i,
- $\Delta x_K := |K|/p_K$: space step of cell K, with $p_K := \sum_{i \in \mathcal{E}_K} |e_i|$ the perimeter of cell K.

4.1. Hyperbolic scheme

In this first section the HLL-DLP scheme from [9] for the homogeneous hyperbolic system (1.2) is recalled then extended to a high-order scheme. First of all, let us recall the classical two points flux (TPF) scheme in 2D:

$$\mathbf{U}_K^{n+1} = \mathbf{U}_K^n - \frac{\Delta t}{|K|} \sum_{i \in \mathcal{E}_K} |e_i| \boldsymbol{\mathcal{F}}(\mathbf{U}_K^n, \mathbf{U}_L^n; \mathbf{n}_{K,i}) \cdot \mathbf{n}_{K,i}, \tag{4.1}$$

where $\boldsymbol{\mathcal{F}}$ is a consistent and conservative two points approximate Riemann solver. Let us underline that the TPF scheme (4.1) is consistent, stable and preserves the set of admissible states $\mathcal{A}$ under the following classical CFL condition:

$$\max_{\substack{K \in \mathcal{M} \\ L \in \mathcal{E}_K}} \left(b_{KL} \frac{\Delta t}{\Delta x_K} \right) \leq 1, \tag{4.2}$$

where b_{KL} is a speed larger than all wave speeds between the states $\mathbf{U}_K$ and $\mathbf{U}_L$.

To get a high-order scheme, we use the MOOD method as in 1D. Indeed, we use the polynomial reconstruction $\widetilde{\mathbf{U}}_K^n(\boldsymbol{x})$ of degree d of the solution on cell K from the MOOD method:

$$\widetilde{\mathbf{U}}_K^n(\boldsymbol{x}) = \mathbf{U}_K^n + \sum_{1 \leq |\boldsymbol{\alpha}| \leq d} \boldsymbol{\mathcal{R}}_K^{\boldsymbol{\alpha}}(\mathbf{U}^n) \left((\boldsymbol{x} - \boldsymbol{x}_K)^{\boldsymbol{\alpha}} - \frac{1}{|K|} \int_K (\boldsymbol{x} - \boldsymbol{x}_K)^{\boldsymbol{\alpha}} d\boldsymbol{x} \right), \tag{4.3}$$

where $\alpha = (\alpha_1, \alpha_2) \in \mathbb{N}^2$ is a multi-index with $|\boldsymbol{\alpha}| = \alpha_1 + \alpha_2$ and as in 1D (2.3) $\boldsymbol{\mathcal{R}}_i^{\boldsymbol{\alpha}}$ are the polynomial coefficients obtained with least-square interpolations from [22]. Then, one can easily get the high-order version of the TPF scheme (4.1) using the polynomial reconstructions:

$$\mathbf{U}_K^{n+1} = \mathbf{U}_K^n - \frac{\Delta t}{|K|} \sum_{i \in \mathcal{E}_K} |e_i| \sum_{r=1}^{R_i} \xi_{ir} \boldsymbol{\mathcal{F}}(\widetilde{\mathbf{U}}_{K,ir}^n, \widetilde{\mathbf{U}}_{L,ir}^n; \mathbf{n}_{K,i}) \cdot \mathbf{n}_{K,i}, \tag{4.4}$$

where ξ_{ir} are the weights of the quadrature rules used on interface i and R_i is the number of quadrature points used for interface i. Besides, $\widetilde{\mathbf{U}}_{K,ir}^n$ is the polynomial reconstruction of the solution in the cell K evaluated at the quadrature points $\boldsymbol{x}_{ir}$: $\widetilde{\mathbf{U}}_{K,ir}^n := \widetilde{\mathbf{U}}_K^n(\boldsymbol{x}_{ir})$. Let us recall that the high-order version of the TPF scheme (4.4) is presented here with a forward Euler time integrator and in order to get a high-order scheme in space and time, one has to use a proper RK time scheme as presented in 1D.

Furthermore, with a classical centered discretization of the source term this scheme does not have the AP property. Besides, the limit scheme is the FV4 scheme which is generally not consistent for unstructured meshes. Whereas, the limit scheme of the HLL-DLP-AP scheme is the Droniou and Le Potier (DLP) scheme for parabolic problems [24], which is consistent and conserve the set of admissible states on any mesh. To get the AP property and conserve the set of admissible states the HLL-DLP-AP scheme has been designed in [9]. As for the TPF scheme, we recall it then we present the high-order version.

Indeed, in the same manner the first-order HLL-DLP scheme developed in [9] is:

$$\mathbf{U}_K^{n+1} = \mathbf{U}_K^n - \frac{\Delta t}{|K|} \sum_{i \in \mathcal{E}_K} |e_i| \sum_{J \in \mathcal{S}_{K,i}} \boldsymbol{\nu}_{K,i}^J(\mathbf{U}^n) \boldsymbol{\mathcal{F}}(\mathbf{U}_K^n, \mathbf{U}_J^n; \boldsymbol{\eta}_{KJ}) \cdot \boldsymbol{\eta}_{KJ}, \tag{4.5}$$

where $\mathcal{S}_{K,i}$ are the set of points used for the reconstruction and $\boldsymbol{\nu}_{K,i}^{J}(\mathbf{U}^n) \geq 0$ are the non-linear coefficients computed in [9] inspired by those used in the DLP scheme for parabolic equations [24]. Lastly, $\boldsymbol{\eta}_{KJ}$ is the unit vector between $\boldsymbol{x}_K$ and $\boldsymbol{x}_J$.

The main advantage of this scheme compared to the TPF flux one is that the numerical diffusion occurs along $\mathbf{n}_{K,i}$ whereas the TPF scheme (4.1) has its numerical diffusion following $\boldsymbol{\eta}_{KL}$. This is one of the key point, to get an AP preserving scheme in 2D with an unstructured mesh. Let us remind, that the HLL-DLP scheme fall back to the TPF scheme when using admissible meshes ($\boldsymbol{\eta}_{KL} = \mathbf{n}_{K,i}$): for instance on Cartesian grids or with Delaunay triangulations.

Then, to get the high-order version of the HLL-DLP scheme (4.5), the polynomial reconstruction $\widetilde{\mathbf{U}}$ (4.3) of the MOOD method is also used:

$$\mathbf{U}_K^{n+1} = \mathbf{U}_K^n - \frac{\Delta t}{|K|} \sum_{i \in \mathcal{E}_K} |e_i| \sum_{r=1}^{R_i} \xi_{ir} \sum_{J \in \mathcal{S}_{K,i}} \boldsymbol{\nu}_{K,i}^{J}(\widetilde{\mathbf{U}}_{ir}^n) \boldsymbol{\mathcal{F}}(\widetilde{\mathbf{U}}_{K,ir}^n, \widetilde{\mathbf{U}}_{J,ir}^n; \boldsymbol{\eta}_{KJ}) \cdot \boldsymbol{\eta}_{KJ}, \tag{4.6}$$

where $\widetilde{\mathbf{U}}_{ir}^n$ is the polynomial reconstruction of the solution on interface i at the right quadrature point. The coefficients $\boldsymbol{\nu}_{K,i}^{J}(\widetilde{\mathbf{U}}_{ir}^n)$ are computed using $\boldsymbol{\mathcal{F}}(\widetilde{\mathbf{U}}_{K,ir}^n, \widetilde{\mathbf{U}}_{J,ir}^n; \boldsymbol{\eta}_{KJ})$, whereas $\boldsymbol{\nu}_{K,i}^{J}(\mathbf{U}^n)$ were computed using $\boldsymbol{\mathcal{F}}(\mathbf{U}_K^n, \mathbf{U}_J^n; \boldsymbol{\eta}_{KJ})$.

Let us underline that the scheme defined by (4.6) is consistent and conservative by construction, as the first-order scheme (4.5). Furthermore, the HLL-DLP scheme (4.5) and its high-order version (4.6) do not preserve the set of admissible states $\mathcal{A}$ on general meshes. Hence, as detailed in [9] the TPF correction still need to be used. This correction consist to use the TPF scheme (4.1) as the last scheme in the MOOD loop since the TPF scheme preserves the set of admissible states $\mathcal{A}$.

Remark 4.1. *Nevertheless, this TPF correction does not delete the AP property of the scheme as in the limit the HLL-DLP-AP and the high-order version give the DLP scheme which conserves the set of admissible states $\mathcal{A}$. Hence, the TPF flux correction is only activated in the transport regime (see [9] for a full proof).*

4.2. Scheme with source term

After this recalling of the HLL-DLP scheme for the homogeneous hyperbolic system (1.2), we now summon up the HLL-DLP-AP scheme with discretization of the source term for the full system (1.1).

As in [26, 6, 9] and as in 1D, the source term is introduced in the numerical flux by using the technique of [7] in order to recover the AP preserving property. Hence, with a general formalism a scheme for the full system (1.1) can be written as:

$$\forall K \in \mathcal{M},\ \mathbf{U}_K^{n+1} = \mathbf{U}_K^n - \frac{\Delta t}{|K|} \sum_{i \in \mathcal{E}_K} |e_i| \overline{\boldsymbol{\mathcal{F}}}_{K,i} \cdot \mathbf{n}_{K,i}, \tag{4.7}$$

where $\overline{\boldsymbol{\mathcal{F}}}_{K,i}$ is a numerical flux that contains the discretization of the source term.

The HLL-DLP-AP scheme with source term from [9] written with the Rusanov flux [48] is:

$$\mathbf{U}_K^{n+1} = \mathbf{U}_K^n - \frac{\Delta t}{|K|}\sum_{i\in\mathcal{E}_K}|e_i|\overline{\boldsymbol{\mathcal{F}}}_{K,i}\cdot\mathbf{n}_{K,i} \tag{4.7}$$

$$\begin{aligned}
&= \mathbf{U}_K^n - \frac{\Delta t}{|K|}\sum_{i\in\mathcal{E}_K}|e_i|\sum_{J\in\mathcal{S}_{K,i}}\boldsymbol{\nu}_{K,i}^J\overline{\boldsymbol{\mathcal{F}}}_{KJ}\cdot\boldsymbol{\eta}_{KJ}\\
&= \mathbf{U}_K^n - \frac{\Delta t}{|K|}\sum_{i\in\mathcal{E}_K}|e_i|\sum_{J\in\mathcal{S}_{K,i}}\boldsymbol{\nu}_{K,i}^J\big(\boldsymbol{\alpha}_{KJ}\boldsymbol{\mathcal{F}}_{KJ}\cdot\boldsymbol{\eta}_{KJ}\\
&\quad - (\boldsymbol{\alpha}_{KJ}-\alpha_{KK})\mathbf{F}(\mathbf{U}_K^n)\cdot\boldsymbol{\eta}_{KJ}\big)\\
&\quad + \frac{\Delta t}{|K|}\sum_{i\in\mathcal{E}_K}|e_i|\sum_{J\in\mathcal{S}_{K,i}}\boldsymbol{\nu}_{K,i}^J(1-\boldsymbol{\alpha}_{KJ})b_{KJ}(\mathbf{R}(\mathbf{U}_K^n)-\mathbf{U}_K^n),
\end{aligned} \tag{4.8}$$

where $\boldsymbol{\nu}_{K,i}^J = (\nu_{K,i}^{J,j})_j$ is obtained as previously on $\boldsymbol{\mathcal{F}}_{KJ}$ (the chosen approximate Riemann solver), with j the index of the equation and b_{KJ} a speed greatest than all wave speeds between the states $\mathbf{U}_K$ and $\mathbf{U}_J$. Moreover, the α coefficients are defined in 2D as (see (2.6) for the 1D definition):

$$\begin{cases}
(\boldsymbol{\alpha}_{KJ})^j &= \alpha_{KJ}^j = \dfrac{b_{KJ}}{b_{KJ}+\gamma_K\delta_{KJ}^j}\in[0;1],\\
\alpha_{KK} &= \dfrac{b_{KK}}{b_{KK}+\gamma_K\delta_{KK}}, \text{ with } \delta_{KK}=\Delta x_K
\end{cases} \tag{4.9}$$

where $\gamma_K = \gamma(\mathbf{U}_K^n)$, and $\delta_{KJ}^j = \dfrac{|K|}{\sum_{i\in\mathcal{E}_K}|e_i|\sum_{J\in\mathcal{S}_{K,i}}\nu_{K,i}^{J,j}}$. Let us underline, that in the case of another two points approximate Riemann solver, such as HLL [35] or even HLLC [57, 58, 3], the definition of the α coefficients and the scheme in (4.8) are slightly different.

The high-order version of the scheme (4.7) is built using the same technique used for the scheme without source term (4.6): each term is evaluated at the quadrature points with the polynomial reconstruction (4.3). Moreover, as in 1D we need to introduce a coefficient β to get the high-order polynomial reconstruction in the transport regime and the first-order one near the diffusive limit. Hence, as in (2.13) we defined β_K^n, with the same properties (2.12) as:

$$\beta_K^n := \frac{\Delta_l}{\Delta_l + \gamma(\mathbf{U}_K^n)t^n\Delta x_K}, \tag{4.10}$$

where $\Delta_l := 5\cdot 10^{-2}L$ is the same characteristic length as in the 1D and $\Delta x_K := \frac{|K|}{p_K}$ is the 2D space step of the cell K. Then, the same definition applies for the convex combination $\overline{\mathbf{U}}$:

$$\overline{\mathbf{U}}_K^n(\boldsymbol{x}) := \beta_K^n\widetilde{\mathbf{U}}_K^n(\boldsymbol{x}) + (1-\beta_K^n)\mathbf{U}_K^n. \tag{4.11}$$

The introduction of this new coefficient in 2D has the same effect as in 1D: the high-order scheme will be used in the transport regime whereas the scheme will go back to first-order near the diffusive limit. The same remarks concerning the use of the first-order scheme when γt increases can be done.

With this new convex combination, we introduce the high-order scheme with source term:

$$\mathbf{U}_K^{n+1} = \mathbf{U}_K^n - \frac{\Delta t}{|K|}\sum_{i\in\mathcal{E}_K}|e_i|\sum_{r=1}^{R_i}\xi_{ir}\sum_{J\in\mathcal{S}_{K,i}}\boldsymbol{\nu}_{K,i}^J(\overline{\mathbf{U}}_{ir}^n)\overline{\boldsymbol{\mathcal{F}}}(\overline{\mathbf{U}}_{K,ir}^n,\overline{\mathbf{U}}_{J,ir}^n;\boldsymbol{\eta}_{KJ})\cdot\boldsymbol{\eta}_{KJ}, \tag{4.12}$$

where $\overline{\boldsymbol{\mathcal{F}}}$ is the numerical flux that includes the discretization of the source term used in (4.7) and $\overline{\mathbf{U}}^n_{K,ir} := \overline{\mathbf{U}}_K(\boldsymbol{x}_{ir})$. Let us recall that the scheme (4.12) is presented with the forward Euler scheme for the time discretization and, when using a high-order time discretization, one needs to write this scheme at each RK step.

As in 1D, the high-order HLL-DLP-AP scheme (4.12) has the AP property as $\beta \xrightarrow[\gamma t\to\infty]{} 0$, which allows to recover the first-order HLL-DLP-AP scheme in the diffusive limit with the same AP correction $\overline{\gamma}$ (see [9] for the details of the computations). Hence, with this AP correction the limit scheme of the high-order HLL-DLP-AP is also the DLP scheme [24].

5. Results in 2D

5.1. Order of the HLL-DLP scheme without source term

Before presenting the results with the source term, some results are presented to tackle with the order of the high-order version of the HLL-DLP scheme (4.6) on some smooth exact solutions. The test is done using the transport equation:

$$\partial_t U + \operatorname{div}(\mathbf{a}U) = 0, \tag{5.1}$$

with the transport at speed $\mathbf{a} = (1\ 1)^T$ of a double sinus $U_0(x,y) = \sin(2\pi x)\sin(2\pi y)$ in the unit square $[0;1]^2$. The square is meshed with an unstructured mesh composed of triangles obtained with Gmsh [27], and each mesh is a refinement of the previous one. In 2D, we use the following definition for the mesh size:

$$\Delta x := \min_{K\in\mathcal{M}} \Delta x_K.$$

Dirichlet boundary conditions are imposed with the exact solution on each side of the square.

The L^2-errors for the high-order HLL-DLP scheme (4.6) with a polynomial reconstruction of degree 0, 1, 2 and 3 are presented at time $t = 1$ in the Table 5. For each computation the appropriate time scheme is used to get the same order in space and time. Hence, as it can be seen the desired order is reached for each polynomial reconstruction.

Mesh		HLL-DLP-$\mathbb{P}_0$		HLL-DLP-$\mathbb{P}_1$		HLL-DLP-$\mathbb{P}_2$		HLL-DLP-$\mathbb{P}_3$	
Nb. cells	Δx	e_{L^2}	p_{L^2}	e_{L^2}	p_{L^2}	e_{L^2}	p_{L^2}	e_{L^2}	p_{L^2}
676	6.45E-03	4.49E-01	—	4.19E-02	—	4.49E-02	—	3.15E-03	—
2 704	3.22E-03	2.86E-01	0.65	8.37E-03	2.32	6.46E-03	2.80	1.86E-04	4.08
10 816	1.61E-03	1.65E-01	0.79	2.24E-03	1.90	8.84E-04	2.87	1.72E-05	3.44
43 264	8.06E-04	8.93E-02	0.89	6.27E-04	1.83	1.22E-04	2.85	1.02E-06	4.07
173 056	4.03E-04	4.66E-02	0.94	1.74E-04	1.85	1.64E-05	2.90	5.91E-08	4.11
692 224	2.01E-04	2.38E-02	0.97	4.97E-05	1.81	2.15E-06	2.93	3.79E-09	3.96

Table 5: Convergence rates with the double sinus

5.2. Order of the HLL-DLP-AP scheme with source term

In order to inspect the order of the HLL-DLP-AP scheme with source term and polynomial reconstruction, we apply the same kind of computations done with the Telegraph equations in 1D to the hyperbolic heat equation (or P_1 model) in 2D:

$$\begin{cases} \partial_t p + \operatorname{div}(\mathbf{u}) & = 0 \\ \partial_t \mathbf{u} + \nabla p & = -\sigma(p, \mathbf{u})\mathbf{u} \end{cases} \tag{5.2}$$

This model also enters in the formalism of the system (1.1) with $\gamma(\mathbf{U}) = \sigma(\mathbf{U})$ and:

$$\mathbf{U} = \begin{pmatrix} p \\ \mathbf{u} \end{pmatrix}, \ \mathbf{F}(\mathbf{U}) = \begin{pmatrix} \mathbf{u}^T \\ p\mathbf{I} \end{pmatrix}, \ \mathbf{R}(\mathbf{U}) = \begin{pmatrix} p \\ 0 \end{pmatrix}. \tag{5.3}$$

Using the exact solutions constructed in Appendix D following the methods from [14, 16], the relative L^2-errors on p are computed for the first-order HLL-DLP-AP and the HLL-DLP-AP with $\mathbb{P}_1$ and $\mathbb{P}_2$ reconstructions limited with the DMP criterion. The DMP limiter is mainly used with low σ and fine meshes, as in those case the high-order scheme is preponderant (see the definition of β (4.10)) and can create spurious oscillations. The results are presented in Tables 6, 7 and 8 for different meshes and three different values of σ. Dirichlet boundary conditions with the exact solution are used on each side of the square.

Mesh		β	HLL-DLP-AP		HLL-DLP-AP-$\mathbb{P}_1$		HLL-DLP-AP-$\mathbb{P}_2$	
Nb. cells	Δx	(4.10)	e_{L^2}	p_{L^2}	e_{L^2}	p_{L^2}	e_{L^2}	p_{L^2}
676	6.45E-03	1.00	3.20E-01	—	9.13E-02	—	9.17E-02	—
2 704	3.22E-03	1.00	1.93E-01	0.73	3.07E-02	1.57	2.95E-02	1.63
10 816	1.61E-03	1.00	1.05E-01	0.88	1.32E-02	1.22	1.42E-02	1.05
43 264	8.06E-04	1.00	5.52E-02	0.93	6.43E-03	1.03	7.21E-03	0.98
173 056	4.03E-04	1.00	2.84E-02	0.96	3.30E-03	0.96	4.05E-03	0.83
692 224	2.01E-04	1.00	1.44E-02	0.98	1.73E-03	0.93	2.70E-03	0.58

Table 6: Convergence rates with $\sigma = 10^{-2}$ and $t = 1$

Mesh		β	HLL-DLP-AP		HLL-DLP-AP-$\mathbb{P}_1$		HLL-DLP-AP-$\mathbb{P}_2$	
Nb. cells	Δx	(4.10)	e_{L^2}	p_{L^2}	e_{L^2}	p_{L^2}	e_{L^2}	p_{L^2}
676	6.45E-03	0.89	3.18E-01	—	1.09E-01	—	1.08E-01	—
2 704	3.22E-03	0.94	1.91E-01	0.73	3.35E-02	1.71	3.17E-02	1.77
10 816	1.61E-03	0.97	1.03E-01	0.89	1.30E-02	1.37	1.36E-02	1.22
43 264	8.06E-04	0.98	5.40E-02	0.93	6.10E-03	1.09	6.75E-03	1.01
173 056	4.03E-04	0.99	2.76E-02	0.97	3.13E-03	0.96	3.86E-03	0.80
692 224	2.01E-04	1.00	1.40E-02	0.98	1.64E-03	0.93	2.53E-03	0.61

Table 7: Convergence rates with $\sigma = 1$ and $t = 1$

The behaviours observed are in the same kind as those observed in 1D with the Telegraph equations in Tables 1, 2 and 3, as the 2D scheme is based on the same construction. Indeed,

Mesh		β	HLL-DLP-AP		HLL-DLP-AP-$\mathbb{P}_1$		HLL-DLP-AP-$\mathbb{P}_2$	
Nb. cells	Δx	(4.10)	e_{L^2}	p_{L^2}	e_{L^2}	p_{L^2}	e_{L^2}	p_{L^2}
676	6.45E-03	0.44	1.08E+00	—	1.49E+00	—	1.48E+00	—
2 704	3.22E-03	0.61	7.38E-01	0.55	8.48E-01	0.82	8.56E-01	0.79
10 816	1.61E-03	0.76	4.23E-01	0.80	4.15E-01	1.03	4.22E-01	1.02
43 264	8.06E-04	0.86	2.25E-01	0.91	2.00E-01	1.06	2.02E-01	1.06
173 056	4.03E-04	0.93	1.15E-01	0.97	9.74E-02	1.04	9.90E-02	1.03
692 224	2.01E-04	0.96	5.81E-02	0.98	4.81E-02	1.02	4.89E-02	1.02

Table 8: Convergence rates with $\sigma = 10$ and $t = 1$

with a small source term, the high-order scheme gives a better precision without reaching the theoretical order of convergence linked to the polynomial reconstruction. Indeed, the scheme with the $\mathbb{P}_1$ reconstruction in the convex combination is better of an order of magnitude whereas the $\mathbb{P}_2$ reconstruction does not lead to smaller errors. Then, when the source term increases, the high-order scheme and first-order scheme are in competition in the convex combination with the β coefficients from (4.10) but for $\sigma = 1$ the high-order scheme is still better than the first-order one. Finally, contrary to the 1D test case, with $\sigma = 10$ in Table 8 the high-order has the same precision as the first-order.

Besides, the coefficient β used in 2D (4.10) is the same as in 1D (2.13) whereas the convergence speeds depend on the dimension of the space [8]. A change of the β coefficients may modify the transition between the polynomial reconstruction and the mean values which will have an impact on the quality of the solution depending of the regime. As a consequence, the quality of the results may be improved if one find a better coefficient β for the 2D case. Let us again remark, contrary to the 1D case, the two schemes have the same precision for $\sigma = 10$, however, the precision is lower with small σ. Moreover, the results are better if one use a more regular mesh but the aim of this scheme is to be used on unstructured meshes.

Remark 5.1. *As in 1D, the test cases are not run for $\sigma \gg 10$ as the numerical computations of the initial solution and the exact solutions are not well defined numerically due to the exponential functions (see Appendix D).*

5.3. Convergence to the diffusion with late time

As in 1D, we now inspect the convergence to the diffusive limit of the high-order scheme, with the same kind of tests.

The first test to check the AP property and the respect of the convergence speeds is made by setting γ and using a final time $t = 100$ as in paragraph 3.3 in 1D. The initial state is a gaussian in density:

$$\rho_0(x, y) = \exp(-(x - 50)^2 - (y - 50)^2) + 1.$$

without any initial speed $\mathbf{u}_0(x, y) = 0$. A coarse mesh of the square $[0; 100]^2$ composed of 2.6×10^4 triangles for a space step of $\Delta x \simeq 9.05 \times 10^{-2}$ is used for this test. As in 1D, in Figures 7 and C.20, the L^2 and L^∞-norms of the density (minus the value at the equilibrium $\rho_E = 1$) and the momentum are plotted over time in Figures 12 and 13 for $\kappa = 1$ and 5. In order to have a better definition of the coefficient β (4.10) with this domain, the characteristic length Δ_l is multiplied by the length of the domain which leads, for this test case, to $\Delta_l := 5$.

Following [8], the expected convergence speeds are in 2D, for $p > 1$:

$$\|\rho - \rho_E\|_{L^p} = \mathcal{O}(1+\gamma t)^{-(1-1/p)}$$
$$\|\rho u\|_{L^p} = \mathcal{O}(1+\gamma t)^{-(1-1/p)-1/2}$$

and as it can be seen in Figures 12 and 13, they are properly satisfied by the two schemes in both norms even if there is small transition needed for the scheme with polynomial reconstruction due to the use of the β coefficient from (4.10).

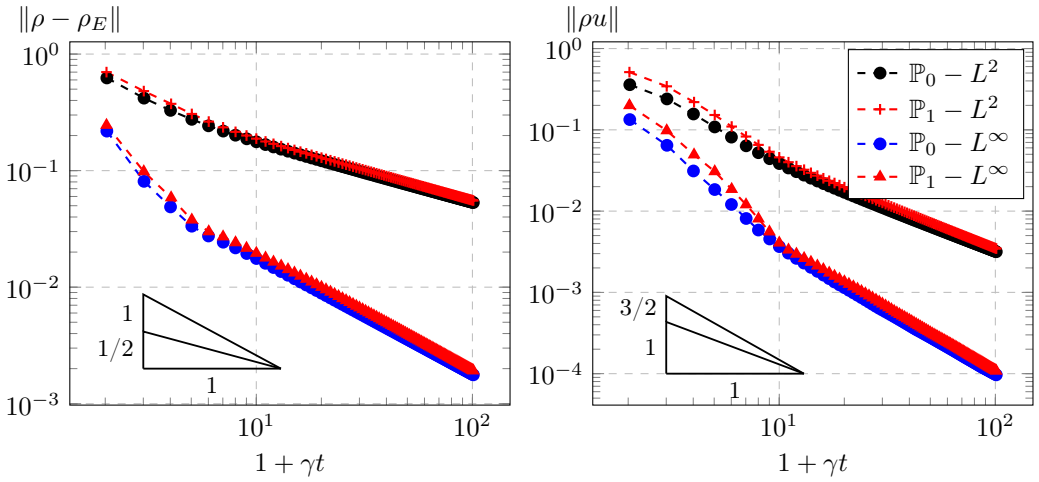

Figure 12: Convergence speeds to the equilibrium in L^2 and L^∞-norms for density and momentum with $\Delta x \simeq 9.05 \times 10^{-2}$ and $\kappa = 1$ in 2D

5.4. Convergence to the diffusion with increasing κt

The next test reaches the limit by increasing γt and the solution obtained by the HLL-DLP-AP scheme (ρ_H) is compared in L^2-norm to the solution (ρ_P) given by the DLP scheme [24] on the limit equation (1.5). On the unit square $[0;1]^2$ meshed with 10^4 triangles for a space step $\Delta x \simeq 1.6 \times 10^{-3}$, the initial condition is given by :

$$\rho_0(x,y) = \frac{1}{10}\left(\exp\left(-\frac{(x-1/2)^2}{2\cdot 0.05^2} - \frac{(y-1/2)^2}{2\cdot 0.05^2}\right) + 1\right),$$

with once again $\mathbf{u}_0(x,y) = 0$. This configuration is similar to the 1D test done in paragraph 3.4.

In Table 9 the results obtained by the scheme with and without reconstruction are presented. The following scheme with a centered discretization of the source term, denoted by HLL-SRC, has also been added to make the comparison with a none AP scheme:

$$\mathbf{U}_K^{n+1} = \mathbf{U}_K^n - \frac{\Delta t}{|K|}\sum_{i\mathcal{E}_K} \boldsymbol{\mathcal{F}}_i + \Delta t\gamma(\mathbf{U}_K^n)\left(\mathbf{R}(\mathbf{U}_K^n) - \mathbf{U}_K^n\right). \tag{5.4}$$

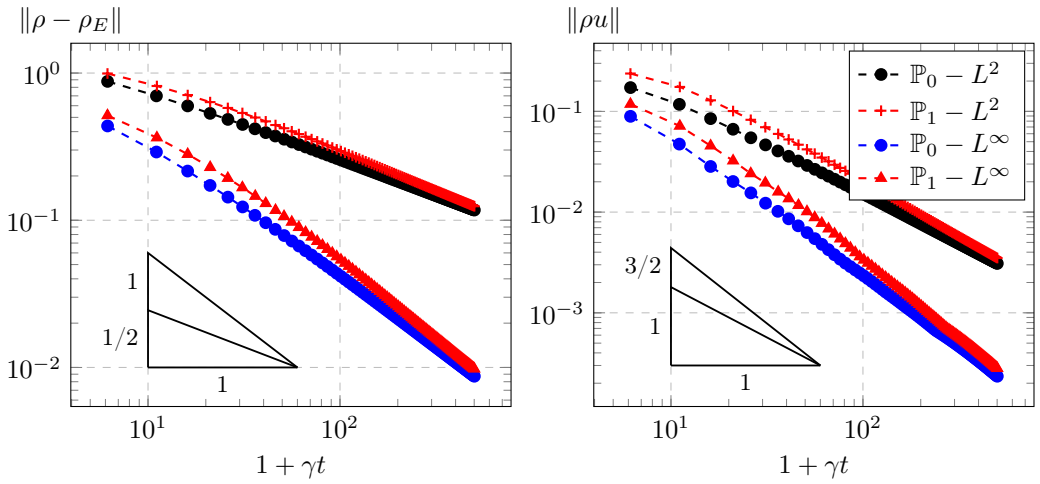

Figure 13: Convergence speeds to the equilibrium in L^2 and L^∞-norms for density and momentum with $\Delta x \simeq 9.05 \times 10^{-2}$ and $\kappa = 5$ in 2D

κ	1	5	25	125	625	3125
t	0.1	0.2	0.4	0.8	1.6	3.2
$\gamma t = \kappa t$	10^{-1}	1	10^1	10^2	10^3	10^4
β (2.13)	9.97E-01	9.69E-01	7.56E-01	2.37E-01	3.01E-02	3.09E-03
Scheme	$\|\rho_P - \rho_H\|_{L^2}$					
HLL-DLP-AP (4.7)	4.11E-03	2.39E-03	1.68E-04	4.56E-05	4.46E-05	2.23E-05
HLL-DLP-AP-$\mathbb{P}_1$ (4.12)	4.52E-03	3.09E-03	1.98E-04	4.01E-04	2.08E-04	3.41E-05
HLL-DLP-AP-$\mathbb{P}_2$ (4.12)	4.49E-03	3.06E-03	1.96E-04	3.63E-04	1.53E-04	2.20E-05
HLL-SRC (5.4)	4.13E-03	3.93E-03	5.14E-03	4.13E-03	5.32E-03	6.43E-03

Table 9: Convergence to the diffusion equation regarding to γt

Let us notice that the three AP scheme converge to the solution of the limit equation, whereas, with the "naïve" scheme (5.4) the norm between the two solutions does not decrease.

Again, from [8] the difference should verify, for all $p > 1$:

$$\|\partial_x^\beta(\rho_P - \rho_H)\|_{L^p} = \mathcal{O}(1+\gamma t)^{-(1-1/p)-\beta/2-1/2}.$$

The results of Table 9 are plotted in Figure 14 in L^2-norm. As in 1D, the convergence speeds are not fully reached. The effect of the β coefficient (4.10) is also clearly seen near $\gamma t \simeq 10$.

5.5. Supersonic step with friction

The next test case is inspired from the step at Mach 3 from [60] with the same computational domain, whereas the isentropic Euler with friction (1.4) is used. Hence, the initialisation is done with $\rho_0 = 1.4$ and $\mathbf{u}_0 = (3\ 0)^T$ and the same value is used for the input flow on the left side of the domain. The right boundary is an outflow with Neumann boundary conditions and the others

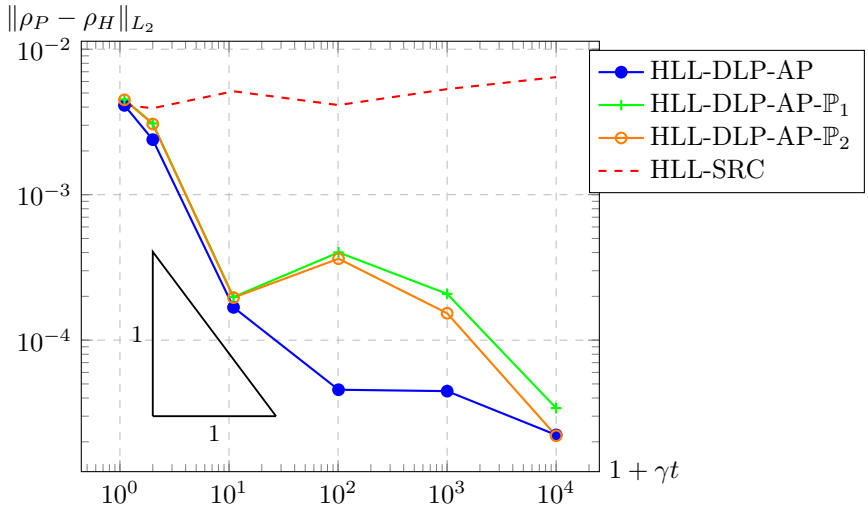

Figure 14: Convergence to the diffusion equation regarding to γt

sides of the step are considered as walls. For the outflow boundary, some large cells (not presented in the results) are added to the computational domain to avoid oscillations leaving the boundary. The friction coefficient follow a nonlinear law : $\kappa(\rho) = 10\left(\frac{\rho}{7}\right)^3$. This friction is chosen in order to have the different regimes in the computations and validate the behaviour of the scheme when γ depends on the solution. Finally, the final time of the simulation is set to $t = 2$.

The density result with the first-order HLL-DLP-AP scheme (4.7) on a fine mesh is presented in Figure 15 and the results for the high-order version (4.12) are presented on coarser meshes in Figures 15 and 16 using a polynomial reconstruction of degree 0, 1, 2 and 3. Let us underline, that the appropriate time schemes are used to get the same order in space and time. For the high-order computations with a polynomial degree of 0, 1, and 2 only the PAD criterion on the density with the TPF correction is used to limit the polynomial reconstruction. The other limiters are not needed in this test case as the left boundary gives the main behaviour and the source term "smoothes" the computations. Whereas, with the fourth-order scheme ($\mathbb{P}_3$), the DMP limiter on the density is needed to get a reasonable solution.

As it can be seen, the high-order schemes give a good solution even on really coarse meshes, and especially near the discontinuities, even if all different regimes are present during the simulation. Moreover, the front discontinuity is not well placed in the coarse mesh of Figure 15 (first-order scheme), compared to the fine mesh in the same figure and the coarse meshes with the high-order scheme in Figure 16.

For the computations with the polynomial reconstruction of degree 0, 1 and 2 the TPF correction is never used and the polynomial degree is decreased on less than 1% percent of the cells. The re-computations and the tests needed by the MOOD paradigm cost less than 1% of the total CPU time. Only the computations with a polynomial reconstruction of degree 3 need the DMP limiter in order to have a good solution. This criterion activates the TPF correction as the first-order scheme with the HLL-DLP-AP flux does not respect the DMP.

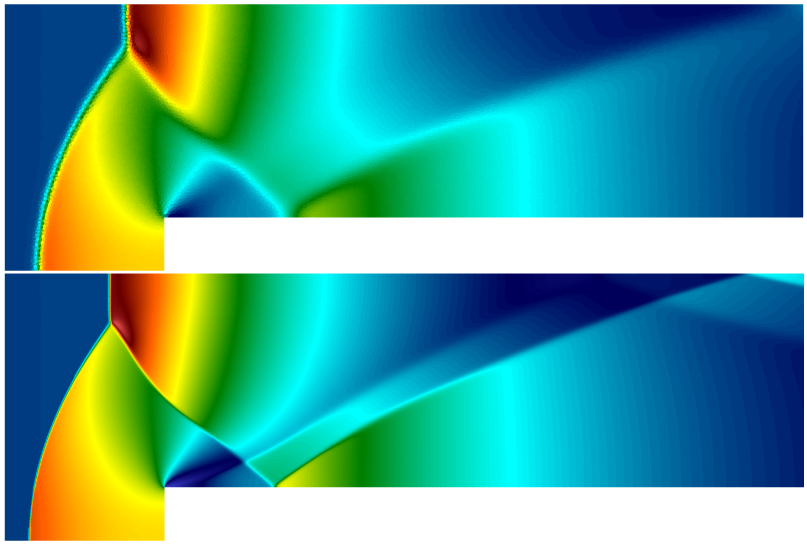

Figure 15: Density results for the step with friction with the first-order scheme on $4 \cdot 10^4$ (top) and 10^6 triangles (bottom)

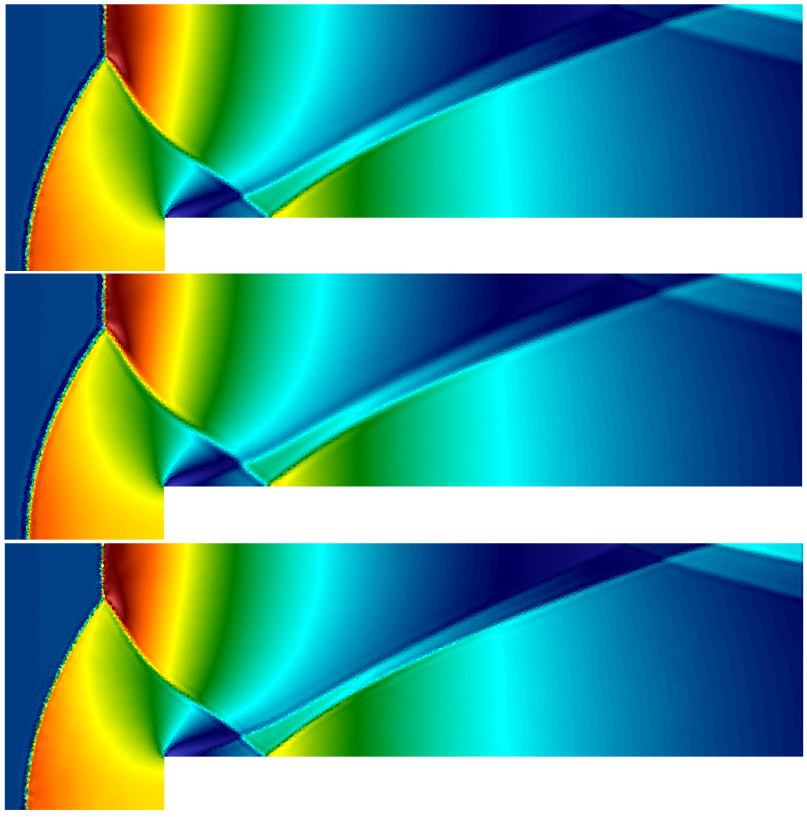

Figure 16: Density results for the step with friction with the high-order schemes on $4 \cdot 10^4$ triangles, from top to bottom : $\mathbb{P}_1$, $\mathbb{P}_2$ and $\mathbb{P}_3$

Regarding to the computational cost, the result on the fine mesh with the first-order HLL-DLP-AP scheme needs 270 hours of CPU time. Whereas, the results for the coarse meshes use only 1, 6, 12 and 24 hours of CPU time for the $\mathbb{P}_0$ to $\mathbb{P}_3$ computations. Hence, it can be clearly seen that the high-order scheme is less expensive in order to have a solution as good as the first-order one on the fine mesh. Besides, the $\mathbb{P}_3$ reconstruction still improves the resolution of the solution near the various reflexions on the left of the domain.

In addition of Figures 15 and 16, we display the polynomial degree and the actual value of the β coefficient (4.10) in Figures 17 and 18. These two figures present the results obtained on the coarse mesh composed of $4 \cdot 10^4$ triangles with the $\mathbb{P}_1$ reconstructions. In Figure 17, it can be seen that the first-order scheme is only used in a very small set of cells, indeed the MOOD loop get back to the $\mathbb{P}_0$ reconstructions on a maximum of 20 cells during the computations. Furthermore, the two-points flulx corrections is never activated. Besides, the figure 17 shows that the scheme with the $\mathbb{P}_1$ reconstruction is mainly used as the coefficient β is near one (4.11).

Figure 17: Map of the polynomial degree at time $t^n = 2$ on $4 \cdot 10^4$ triangles (blue: $\mathbb{P}_1$, red: $\mathbb{P}_0$)

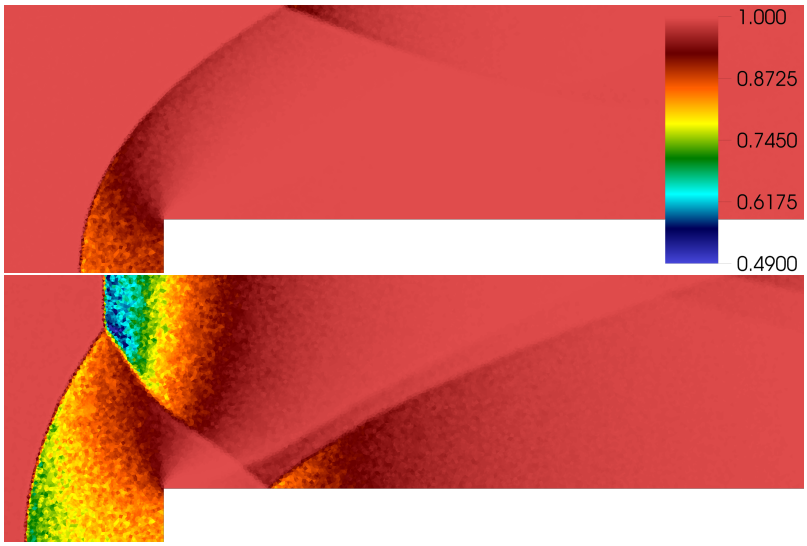

Figure 18: Value of the β coefficient (4.10) at time $t^n = 1.2$ and 2 with the $\mathbb{P}_1$ reconstruction on $4 \cdot 10^4$ triangles

Within the various configurations tested the high-order version of the HLL-DLP-AP scheme has the behaviour expected: the AP property and the set of admissible states are conserved. Moreover, the accuracy is improved even though the scheme degenerates to order one in the diffusive regime.

Conclusion, extensions

With this work, we provide a high-order extension for asymptotic preserving schemes adapted to system of conservation laws with source term (1.1) in 1D [7] and 2D [9]. This extension was done using a convex combination between a polynomial reconstruction of the solution and the mean values to preserve the AP property. Some reference solutions were proposed to study the high-order schemes regarding to the different scales of γt using continuous or discontinuous solutions. These tests lead to the conclusion that the scheme is more accurate within the transport regime and that the classical first order scheme is reached when γt increases. Besides, the scheme is always AP as the first scheme (HLL-AP or HLL-DLP-AP) preserves this behaviour. The set of admissible states is conserved with the high-order scheme thanks to the *a posteriori* limitation of the MOOD method [19].

For now the scheme is not uniformly high-order but as it can be seen in the various results and especially on the step with friction in Figure 16, that the polynomial reconstruction greatly improves the solution in the transport regime. Let us remark, as it was already said for both the 1D and 2D cases, the fact that the scheme is not high-order near the diffusive limit is not preponderant as the phenomena are slow for large γ in this case. As a consequence, one of the main outlook for this work is to create a full high-order and AP scheme by modifying the α coefficients (2.6)-(4.9) to obtain the properties described in (2.10) to get ride of the convex combination with the β coefficients (2.13)-(4.10)

Acknowledgments

The authors were funded by the ANR project ACHYLLES (grant number ANR-14-CE25-0001).

References

[1] U. M. Ascher, S. J. Ruuth, and R. J. Spiteri. Implicit-explicit Runge-Kutta methods for time-dependent partial differential equations. *Appl. Numer. Math.*, 25(2-3):151–167, 1997. Special issue on time integration (Amsterdam, 1996).

[2] M. Ben-Artzi and J. Falcovitz. *Generalized Riemann problems in computational fluid dynamics*, volume 11 of *Cambridge Monographs on Applied and Computational Mathematics*. Cambridge University Press, Cambridge, 2003.

[3] C. Berthon, P. Charrier, and B. Dubroca. An HLLC scheme to solve the M_1 model of radiative transfer in two space dimensions. *J. Sci. Comput.*, 31(3):347–389, 2007.

[4] C. Berthon and V. Desveaux. An entropy preserving MOOD scheme for the Euler equations. *Int. J. Finite Vol.*, 11:39, 2014.

[5] C. Berthon, P. G. LeFloch, and R. Turpault. Late-time/stiff-relaxation asymptotic-preserving approximations of hyperbolic equations. *Math. Comp.*, 82(282):831–860, 2013.

[6] C. Berthon, G. Moebs, C. Sarazin-Desbois, and R. Turpault. An asymptotic-preserving scheme for systems of conservation laws with source terms on 2D unstructured meshes. *Commun. Appl. Math. Comput. Sci.*, 11(1):55–77, 2016.

[7] C. Berthon and R. Turpault. Asymptotic preserving HLL schemes. *Numer. Methods Partial Differential Equations*, 27(6):1396–1422, 2011.

[8] S. Bianchini, B. Hanouzet, and R. Natalini. Asymptotic behavior of smooth solutions for partially dissipative hyperbolic systems with a convex entropy. *Comm. Pure Appl. Math.*, 60(11):1559–1622, 2007.

[9] F. Blachère and R. Turpault. An admissibility and asymptotic-preserving scheme for systems of conservation laws with source term on 2D unstructured meshes. *J. Comput. Phys.*, 315:98–123, 2016.

[10] S. Boscarino, P. G. LeFloch, and G. Russo. High-order asymptotic-preserving methods for fully nonlinear relaxation problems. *SIAM J. Sci. Comput.*, 36(2):A377–A395, 2014.

[11] S. Boscarino, L. Pareschi, and G. Russo. Implicit-explicit Runge-Kutta schemes for hyperbolic systems and kinetic equations in the diffusion limit. *SIAM J. Sci. Comput.*, 35(1):A22–A51, 2013.

[12] W. Boscheri, R. Loubère, and M. Dumbser. Direct arbitrary-Lagrangian-Eulerian ADER-MOOD finite volume schemes for multidimensional hyperbolic conservation laws. *J. Comput. Phys.*, 292:56–87, 2015.

[13] C. Buet, B. Després, and E. Franck. An asymptotic preserving scheme with the maximum principle for the M_1 model on distorded meshes. *C. R. Math. Acad. Sci. Paris*, 350(11-12):633–638, 2012.

[14] C. Buet, B. Després, and E. Franck. Design of asymptotic preserving finite volume schemes for the hyperbolic heat equation on unstructured meshes. *Numer. Math.*, 122(2):227–278, 2012.

[15] C. Buet, B. Després, and E. Franck. Asymptotic preserving schemes on distorted meshes for Friedrichs systems with stiff relaxation: application to angular models in linear transport. *J. Sci. Comput.*, 62(2):371–398, 2015.

[16] C. Buet, B. Després, E. Franck, and T. Leroy. Proof of uniform convergence for a cell-centered AP discretization of the hyperbolic heat equation on general meshes. *Mathematics of Computation*, 2016.

[17] S. Chen, X. Han, and H. Zhang. The generalized Riemann problem for first order quasilinear hyperbolic systems of conservation laws. II. *Acta Appl. Math.*, 108(2):235–277, 2009.

[18] S. Chen, D. Huang, and X. Han. The generalized Riemann problem for first order quasilinear hyperbolic systems of conservation laws. I. *Bull. Korean Math. Soc.*, 46(3):409–434, 2009.

[19] S. Clain, S. Diot, and R. Loubère. A high-order finite volume method for systems of conservation laws—Multi-dimensional Optimal Order Detection (MOOD). *J. Comput. Phys.*, 230(10):4028–4050, 2011.

[20] S. Clain and J. Figueiredo. The MOOD method for the non-conservative shallow-water system. October 2014.

[21] G. Dahlquist. Convergence and stability in the numerical integration of ordinary differential equations. *Math. Scand.*, 4:33–53, 1956.

[22] S. Diot, S. Clain, and R. Loubère. Improved detection criteria for the multi-dimensional optimal order detection (MOOD) on unstructured meshes with very high-order polynomials. *Comput. & Fluids*, 64:43–63, 2012.

[23] S. Diot, R. Loubère, and S. Clain. The multidimensional optimal order detection method in the three-dimensional case: very high-order finite volume method for hyperbolic systems. *Internat. J. Numer. Methods Fluids*, 73(4):362–392, 2013.

[24] J. Droniou and C. Le Potier. Construction and convergence study of schemes preserving the elliptic local maximum principle. *SIAM J. Numer. Anal.*, 49(2):459–490, 2011.

[25] B. Dubroca and J. Feugeas. Theoretical and numerical study of a moment closure hierarchy for the radiative transfer equation. *C. R. Acad. Sci. Paris Sér. I Math.*, 329(10):915–920, 1999.

[26] A. Duran, F. Marche, R. Turpault, and C. Berthon. Asymptotic preserving scheme for the shallow water equations with source terms on unstructured meshes. *J. Comput. Phys.*, 287:184–206, 2015.

[27] C. Geuzaine and J.-F. Remacle. Gmsh: A 3-D finite element mesh generator with built-in pre- and post-processing facilities. *Internat. J. Numer. Methods Engrg.*, 79(11):1309–1331, 2009.

[28] S. Goldstein. On diffusion by discontinuous movements, and on the telegraph equation. *Quart. J. Mech. Appl. Math.*, 4:129–156, 1951.

[29] L. Gosse and G. Toscani. An asymptotic-preserving well-balanced scheme for the hyperbolic heat equations. *C. R. Math. Acad. Sci. Paris*, 334(4):337–342, 2002.

[30] S. Gottlieb. On high order strong stability preserving Runge-Kutta and multi step time discretizations. *J. Sci. Comput.*, 25(1-2):105–128, 2005.

[31] S. Gottlieb and C.-W. Shu. Total variation diminishing Runge-Kutta schemes. *Math. Comp.*, 67(221):73–85, 1998.

[32] S. Gottlieb, C.-W. Shu, and E. Tadmor. Strong stability-preserving high-order time discretization methods. *SIAM Rev.*, 43(1):89–112, 2001.

[33] B. Hanouzet and R. Natalini. Global existence of smooth solutions for partially dissipative hyperbolic systems with a convex entropy. *Arch. Ration. Mech. Anal.*, 169(2):89–117, 2003.

[34] A. Harten, B. Engquist, S. Osher, and S. R. Chakravarthy. Uniformly high-order accurate essentially nonoscillatory schemes. III. *J. Comput. Phys.*, 71(2):231–303, 1987.

[35] A. Harten, P. D. Lax, and B. van Leer. On upstream differencing and Godunov-type schemes for hyperbolic conservation laws. *SIAM Rev.*, 25(1):35–61, 1983.

[36] F. Huang, P. Marcati, and R. Pan. Convergence to the Barenblatt solution for the compressible Euler equations with damping and vacuum. *Arch. Ration. Mech. Anal.*, 176(1):1–24, 2005.

[37] W. Hundsdorfer, S. J. Ruuth, and R. J. Spiteri. Monotonicity-preserving linear multistep methods. *SIAM J. Numer. Anal.*, 41(2):605–623, 2003.

[38] J. Jang, F. Li, J.-M. Qiu, and T. Xiong. High order asymptotic preserving DG-IMEX schemes for discrete-velocity kinetic equations in a diffusive scaling. *J. Comput. Phys.*, 281:199–224, 2015.

[39] G.-S. Jiang and C.-W. Shu. Efficient implementation of weighted ENO schemes. *J. Comput. Phys.*, 126(1):202–228, 1996.

[40] S. Jin. Efficient asymptotic-preserving (AP) schemes for some multiscale kinetic equations. *SIAM J. Sci. Comput.*, 21(2):441–454 (electronic), 1999.

[41] D. I. Ketcheson and A. C. Robinson. On the practical importance of the SSP property for Runge-Kutta time integrators for some common Godunov-type schemes. *Int. J. Numer. Methods Fluids*, 48(3):271–303, 2005.

[42] E. J. Kubatko, B. A. Yeager, and D. I. Ketcheson. Optimal strong-stability-preserving Runge-Kutta time discretizations for discontinuous Galerkin methods. *J. Sci. Comput.*, 60(2):313–344, 2014.

[43] P. Lafitte, A. Lejon, and G. Samaey. A High-Order Asymptotic-Preserving Scheme for Kinetic Equations Using Projective Integration. *SIAM J. Numer. Anal.*, 54(1):1–33, 2016.

[44] H. W. J. Lenferink. Contractivity-preserving implicit linear multistep methods. *Math. Comp.*, 56(193):177–199, 1991.

[45] X.-D. Liu, S. Osher, and T. Chan. Weighted essentially non-oscillatory schemes. *J. Comput. Phys.*, 115(1):200–212, 1994.

[46] R. Loubère, M. Dumbser, and S. Diot. A new family of high order unstructured MOOD and ADER finite volume schemes for multidimensional systems of hyperbolic conservation laws. *Commun. Comput. Phys.*, 16(3):718–763, 2014.

[47] P. Marcati and A. Milani. The one-dimensional Darcy's law as the limit of a compressible Euler flow. *J. Differential Equations*, 84(1):129–147, 1990.

[48] V. V. Rusanov. The calculation of the interaction of non-stationary shock waves with barriers. *Ž. Vyčisl. Mat. i Mat. Fiz.*, 1:267–279, 1961.

[49] S. J. Ruuth. Global optimization of explicit strong-stability-preserving Runge-Kutta methods. *Math. Comp.*, 75(253):183–207 (electronic), 2006.

[50] S. J. Ruuth and R. J. Spiteri. High-order strong-stability-preserving Runge-Kutta methods with downwind-biased spatial discretizations. *SIAM J. Numer. Anal.*, 42(3):974–996, 2004.

[51] C.-W. Shu. Total-variation-diminishing time discretizations. *SIAM J. Sci. Statist. Comput.*, 9(6):1073–1084, 1988.

[52] C.-W. Shu and S. Osher. Efficient implementation of essentially nonoscillatory shock-capturing schemes. *J. Comput. Phys.*, 77(2):439–471, 1988.

[53] R. J. Spiteri and S. J. Ruuth. A new class of optimal high-order strong-stability-preserving time discretization methods. *SIAM J. Numer. Anal.*, 40(2):469–491 (electronic), 2002.

[54] R. J. Spiteri and S. J. Ruuth. Non-linear evolution using optimal fourth-order strong-stability-preserving Runge-Kutta methods. *Math. Comput. Simulation*, 62(1-2):125–135, 2003.

[55] G. I. Taylor. Diffusion by continuous movements. *Proceedings of the London Mathematical Society*, s2-20(1):196–212, 1922.

[56] V. A. Titarev and E. F. Toro. ADER: arbitrary high order Godunov approach. In *Proceedings of the Fifth International Conference on Spectral and High Order Methods (ICOSAHOM-01) (Uppsala)*, volume 17, pages 609–618, 2002.

[57] E. F. Toro. *Riemann solvers and numerical methods for fluid dynamics*. Springer-Verlag, Berlin, third edition, 2009. A practical introduction.

[58] E. F. Toro, M. Spruce, and W. Speares. Restoration of the contact surface in the HLL-Riemann solver. *Shock Waves*, 4(1):25–34, 1994.

[59] B. van Leer. Towards the ultimate conservative difference scheme. V. A second-order sequel to Godunov's method. *J. Comput. Phys.*, 32:101–136, 1979.

[60] P. Woodward and P. Colella. The numerical simulation of two-dimensional fluid flow with strong shocks. *J. Comput. Phys.*, 54(1):115–173, 1984.

A. Reference solution for 1D Riemann problems for Telegraph equations

The aim is to find reference solutions to Riemann problems associated to the system (3.1) with the following initial condition (see also Figure A.19):

$$\mathbf{U}(t=0,x) = \begin{cases} \mathbf{U}_L & \text{if } x < 0, \\ \mathbf{U}_R & \text{otherwise.} \end{cases} \tag{A.1}$$

The reader is referred to [18, 17] for a full proof of the structure of the Riemann problem with source term described in Figure A.19 and used in the next parts.

Then, reference solutions are build in the upcoming parts. The construction is done first in the left and right zones of the Riemann problem then, using two different methods for the central zone.

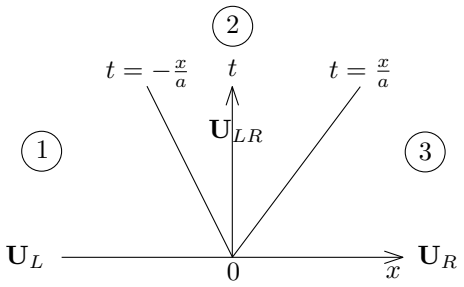

Figure A.19: Structure and zones of the Riemann problem

A.1. Solution in the left and right zones

Firstly, the left and right zones (zones 1 and 3 in Figure A.19) are treated in the same manner. In this part the mean free path σ may be discontinuous across the initial interface ($x = 0$):

$$\sigma := \sigma(x) = \begin{cases} \sigma_L & \text{if } x < 0 \\ \sigma_R & \text{otherwise.} \end{cases} \tag{A.2}$$

In these zones of the Riemann problem, the system (3.1) is reduced to:

$$\left\{ \begin{array}{rcl} \partial_t u &=& \sigma(v-u) \\ \partial_t v &=& \sigma(u-v) \end{array} \right. \iff \left\{ \begin{array}{rcl} \partial_t(u+v) &=& 0 \\ \partial_t(u-v) &=& -2\sigma(u-v) \end{array} \right. ,$$

which leads for zone 1:

$$\left\{ \begin{array}{rcl} u_1(t) &=& \frac{1}{2}\left((u_L+v_L)+(u_L-v_L)e^{-2\sigma_L t}\right) \\ v_1(t) &=& \frac{1}{2}\left((u_L+v_L)+(v_L-u_L)e^{-2\sigma_L t}\right) \end{array} \right. , \tag{A.3}$$

and for zone 3:

$$\left\{ \begin{array}{rcl} u_3(t) &=& \frac{1}{2}\left((u_R+v_R)+(u_R-v_R)e^{-2\sigma_R t}\right) \\ v_3(t) &=& \frac{1}{2}\left((u_R+v_R)+(v_R-u_R)e^{-2\sigma_R t}\right) \end{array} \right. . \tag{A.4}$$

For the central zone, some preliminary computations are needed, and two methods are presented in the two following paragraphs.

A.2. Central zone, method 1: substitution

The first method presented uses a reformulation of the initial system (3.1) and a finite difference scheme on the reformulated system to get the solution in the central zone (zone 2 in Figure A.19). This method assumes that σ is constant over the whole area, hence: $\sigma := \sigma_L = \sigma_R$.

The following substitutions are done to reduce the system (3.1) and rotate the central zone:

$$\left\{ \begin{array}{rcl} u &\leftarrow& e^{-\sigma t}\bar{u} \\ v &\leftarrow& e^{-\sigma t}\bar{v} \end{array} \right. \text{ and } \left\{ \begin{array}{rcl} y &\leftarrow& at + x \\ s &\leftarrow& at - x \end{array} \right. ,$$

which leads to:

$$\left\{ \begin{array}{rcl} 2a\partial_y \bar{u} &=& \sigma\bar{v} \\ 2a\partial_s \bar{v} &=& \sigma\bar{u} \end{array} \right. . \tag{A.5}$$

Where the boundary condition is known for $\bar{u}$ at the interface $t = -\frac{x}{a}$ $(y = 0)$, since u is continuous across the interface between zone 1 and 2. For $\bar{v}$, the boundary condition is located at the interface $t = \frac{x}{a}$ $(s = 0)$:

$$\left\{ \begin{array}{rcl} \bar{u}(y=0,s) & = & e^{\sigma t} u_1(t) \\ \bar{v}(y,s=0) & = & e^{\sigma t} v_3(t) \end{array} \right. , \tag{A.6}$$

with $t = \frac{1}{2a}(y + s)$. The other sides of the computational domain remain open. In order to get a solution to the problem (A.5)-(A.6) an explicit finite difference scheme is set up, with the following discretization:

$$\left\{ \begin{array}{rcl} \forall i \in \mathbb{N}, y_i & = & i\Delta \\ \forall j \in \mathbb{N}, s_j & = & j\Delta \end{array} \right. \text{ and } \left\{ \begin{array}{rcl} \bar{u}_{i,j} & := & \bar{u}(y_i, s_j) \\ \bar{v}_{i,j} & := & \bar{v}(y_i, s_j) \end{array} \right. .$$

Finally, a finite difference scheme for this problem is:

$$\left\{ \begin{array}{ll} \forall i \in \mathbb{N}, \forall j \in \mathbb{N}, \bar{u}_{i+1,j} & = \bar{u}_{i,j} + \frac{\sigma\Delta}{2a} \bar{v}_{i,j} \\ \forall j \in \mathbb{N}, \forall i \in \mathbb{N}, \bar{v}_{i,j+1} & = \bar{v}_{i,j} + \frac{\sigma\Delta}{2a} \bar{u}_{i,j} \end{array} \right. . \tag{A.7}$$

A.3. Central zone, method 2: power series

The second method uses a power series decomposition of u and v, with $y := \frac{x}{t}$:

$$\left\{ \begin{array}{rcl} u(t,x) & = & \sum_{i=0}^{\infty} \phi_i(y) t^i \\ v(t,x) & = & \sum_{i=0}^{\infty} \psi_i(y) t^i \end{array} \right. . \tag{A.8}$$

The advantages of this method over the first one is that the mean free path σ may be discontinuous in the central zone (zone 2 in Figure A.19) as in (A.2). Introducing the power series of (A.8) into (3.1) and grouping the different powers of t leads to:

$$\left\{ \begin{array}{rcl} (a-y)\phi_0' + \sum_{i=1}^{\infty} \left((a-y)\phi_i' + i\phi_i - \sigma\left(\psi_{i-1} - \phi_{i-1}\right) \right) t^i & = & 0 \\ -(a+y)\psi_0' + \sum_{i=1}^{\infty} \left(-(a+y)\psi_i' + i\psi_i - \sigma\left(\phi_{i-1} - \psi_{i-1}\right) \right) t^i & = & 0 \end{array} \right. .$$

Isolating the term in t^0, and using the appropriate initial conditions gives:

$$\left\{ \begin{array}{rcl} \phi_0 & = & u_L \\ \psi_0 & = & v_R \end{array} \right. .$$

Then for a general $i > 1$, we have:

$$\left\{ \begin{array}{rcl} \phi_i' & = & \frac{1}{a-y} \left(\sigma\left(\psi_{i-1} - \phi_{i-1}\right) - i\phi_i \right) \\ \psi_i' & = & \frac{-1}{a+y} \left(\sigma\left(\phi_{i-1} - \psi_{i-1}\right) - i\psi_i \right) \end{array} \right. . \tag{A.9}$$

The previous ODEs are solved numerically, using a classical explicit scheme:

$$\left\{ \begin{array}{rcl} \phi_{i,j+1} & = & \phi_{i,j} + \frac{\Delta y}{a-y} \left(\sigma\left(\psi_{i-1,j} - \phi_{i-1,j}\right) - i\phi_{i,j} \right) \\ \psi_{i,j+1} & = & \psi_{i,j} + \frac{-\Delta y}{a+y} \left(\sigma\left(\phi_{i-1,j} - \psi_{i-1,j}\right) - i\psi_{i,j} \right) \end{array} \right. , \tag{A.10}$$

with the following discretization: $\phi_{i,j} := \phi_i(j\Delta y)$ and $\psi_{i,j} := \psi_i(j\Delta y)$, where $\Delta y := \frac{\Delta x}{t}$. Those ODEs are valid only in zone 2, hence, $j \in [\![N_1; N_3]\!]$, where $x_{\min} + N_1\Delta x = -at$ (beginning of zone 2) and $x_{\min} + N_3\Delta x = at$ (end of zone 2) in the domain $[x_{\min}; x_{\max}]$. The initial conditions are extracted from the power series decomposition of (A.3)-(A.4):

$$\begin{cases} \phi_{i,N_1} &= \frac{1}{2}(u_L - v_L)\frac{(-2\sigma_L)^i}{i!} \quad (y = -a) \\ \psi_{i,N_3} &= \frac{1}{2}(v_R - u_R)\frac{(-2\sigma_R)^i}{i!} \quad (y = a) \end{cases}.$$

B. Smooth solutions in 1D

We now present the construction of smooth solutions for the Telegraph equations (3.1). Following the method used for the hyperbolic heat equation in [14, 16] they can be expressed as:

$$\begin{cases} u(t,x) &= f(t,x) + \frac{1}{2\sigma}\partial_t f(t,x) - \frac{a}{2\sigma}\partial_x f(t,x) \\ v(t,x) &= f(t,x) + \frac{1}{2\sigma}\partial_t f(t,x) + \frac{a}{2\sigma}\partial_x f(t,x) \end{cases}, \tag{B.1}$$

where f is a solution of the following PDE:

$$2\sigma\partial_t f(t,x) + \partial_t^2 f(t,x) - a^2\partial_x^2 f(t,x) = 0. \tag{B.2}$$

For instance, with a separation of variables, a solution of (B.2) can be expressed as: $f(x,t) = \alpha(t)\cos(2\pi x)$, with $\alpha(t)$ solution of this ODE:

$$4\pi^2 a^2\alpha(t) + 2\sigma\alpha'(t) + \alpha''(t) = 0.$$

Hence, depending on the sign of $\sigma - 2\pi a$, three solutions are proposed. For $0 < \sigma < 2\pi a$, a solution reads as:

$$\alpha(t) = e^{-\sigma t}\left(\sin\left(\sqrt{4\pi^2a^2 - \sigma^2}t\right) + \cos\left(\sqrt{4\pi^2a^2 - \sigma^2}t\right)\right) \tag{B.3}$$

Then, for $\sigma = 2\pi a$, a solution is:

$$\alpha(t) = \exp(-2\pi a t)(1 + t) \tag{B.4}$$

Finally, for $\sigma > 2\pi a$, the computations leads to:

$$\alpha(t) = \exp\left(-(\sigma - \sqrt{\sigma^2 - 4\pi^2a^2})t\right) + \exp\left(-(\sigma + \sqrt{\sigma^2 - 4\pi^2a^2})t\right) \tag{B.5}$$

Then using one of the expression from (B.3), (B.4) or (B.5), the expression of f and (B.1), it is possible to compute a smooth and exact solution of (3.1).

C. Convergence speeds in 1D

The rates of convergence to the diffusion limit with $\kappa = 5$ are presented in the Figures C.20 to C.22. For the description of this test case the reader is referred to the description done with $\kappa = 1$ linked to the results in Figures 7 to 9.

The theoretical rates from [8] are respected for the space and time derivatives of the density and the momentum. Only the second time derivatives show some oscillations due to the method used for the numerical derivations.

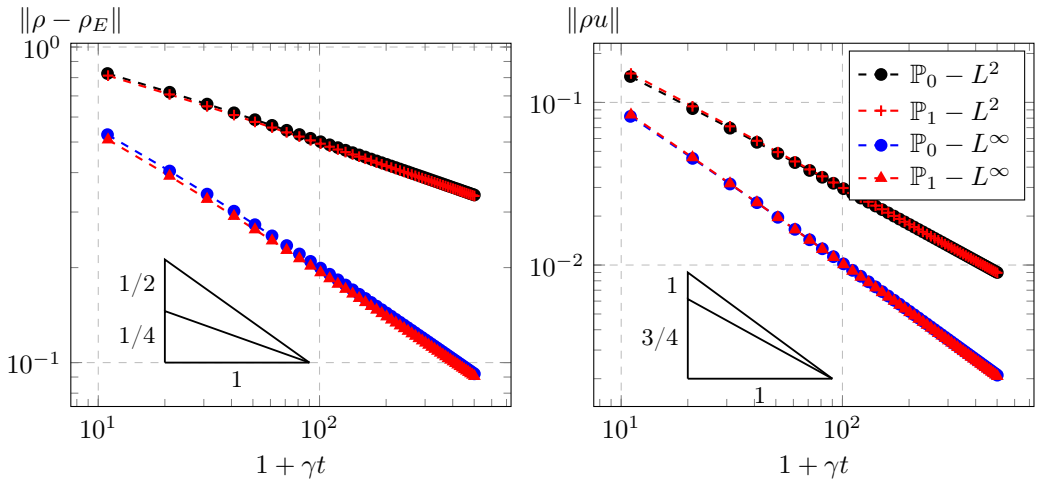

Figure C.20: Convergence speeds to the equilibrium in L^2 and L^∞-norms for density and momentum with $\Delta x = 5 \times 10^{-2}$ and $\kappa = 5$ in 1D

D. Smooth solutions in 2D

Again, by following the same method from [14, 16] already used in 1D with the Telegraph equations (3.1), three exact solutions can also be exhibited on the unit square $[0;1]^2$ with different σ for the hyperbolic heat equation (5.2). Those solutions can be expressed as:

$$\begin{cases} p(t,\boldsymbol{x}) & = f(t,\boldsymbol{x}) + \dfrac{1}{\sigma}\partial_t f(t,\boldsymbol{x}) \\ \mathbf{u}(t,\boldsymbol{x}) & = -\dfrac{1}{\sigma}\nabla f(t,\boldsymbol{x}) \end{cases},$$

with, f solution of the following PDE:

$$\sigma\partial_t f(t,\boldsymbol{x}) + \partial_t^2 f(t,\boldsymbol{x}) - \Delta f(t,\boldsymbol{x}) = 0.$$

Then, for instance, f can be chosen such that: $f(t,\boldsymbol{x}) = \alpha(t)\cos(2\pi x)\cos(2\pi y)$. In this case, $\alpha(t)$ is solution of this ODE:

$$\sigma\alpha'(t) + \alpha''(t) - 4\pi^2\alpha(t) = 0.$$

Hence, a first solution is, for $0 < \sigma < \sqrt{32}\pi$:

$$\alpha(t) = \exp\left(\frac{-\sigma t}{2}\right)\left(\sin\left(\frac{\sqrt{32\pi^2 - \sigma^2}t}{2}\right) + \cos\left(\frac{\sqrt{32\pi^2 - \sigma^2}t}{2}\right)\right).$$

Then, for $\sigma = \sqrt{32}\pi$, the computations gives:

$$\alpha(t) = \exp\left(-2\sqrt{2}\pi t\right)(1+t).$$

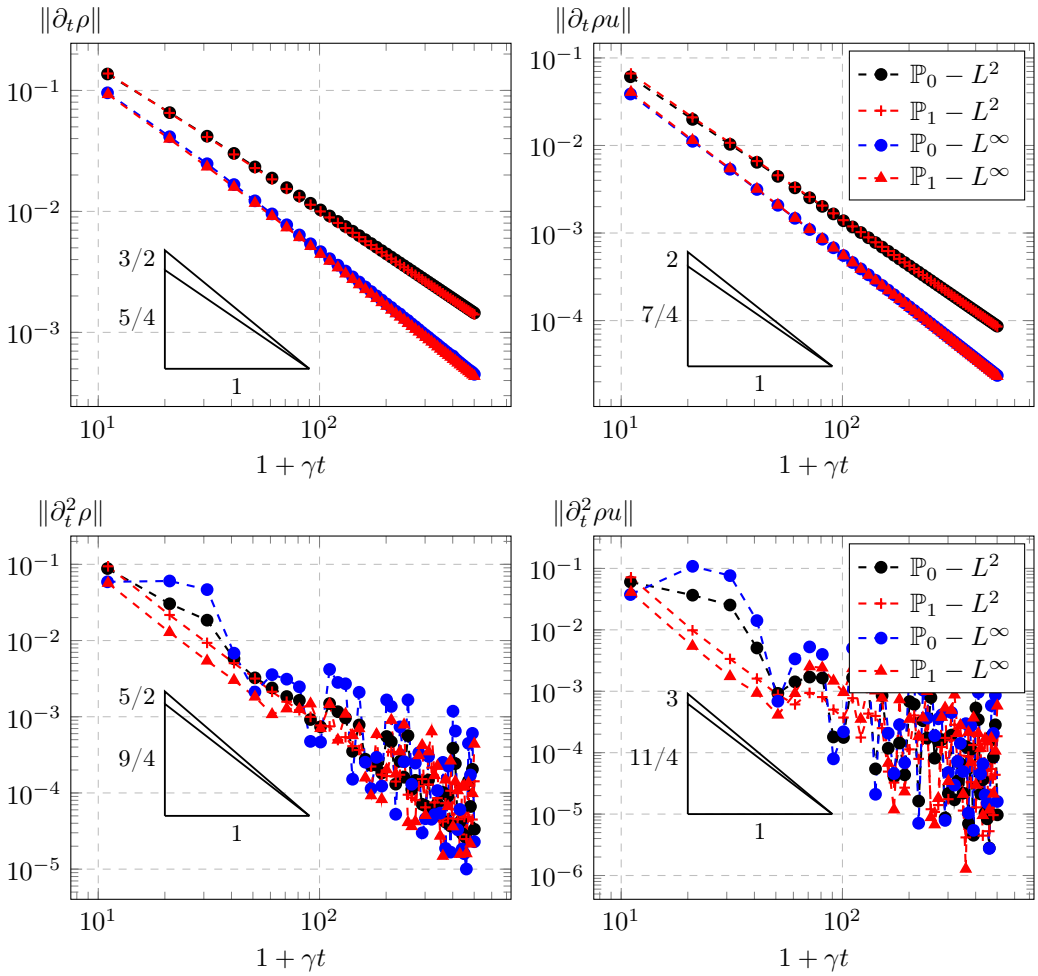

Figure C.21: Convergence speeds to the equilibrium in L^2 and L^∞-norms for the time derivatives of the density and momentum with $\Delta x = 5 \times 10^{-2}$ and $\kappa = 5$ in 1D

Finally for $\sigma > \sqrt{32}\pi$, $\alpha(t)$ can be defined as:

$$\alpha(t) = \exp\left(\frac{-\sigma + \sqrt{\sigma^2 - 32\pi^2}}{2} t\right) + \exp\left(\frac{-\sigma - \sqrt{\sigma^2 - 32\pi^2}}{2} t\right).$$

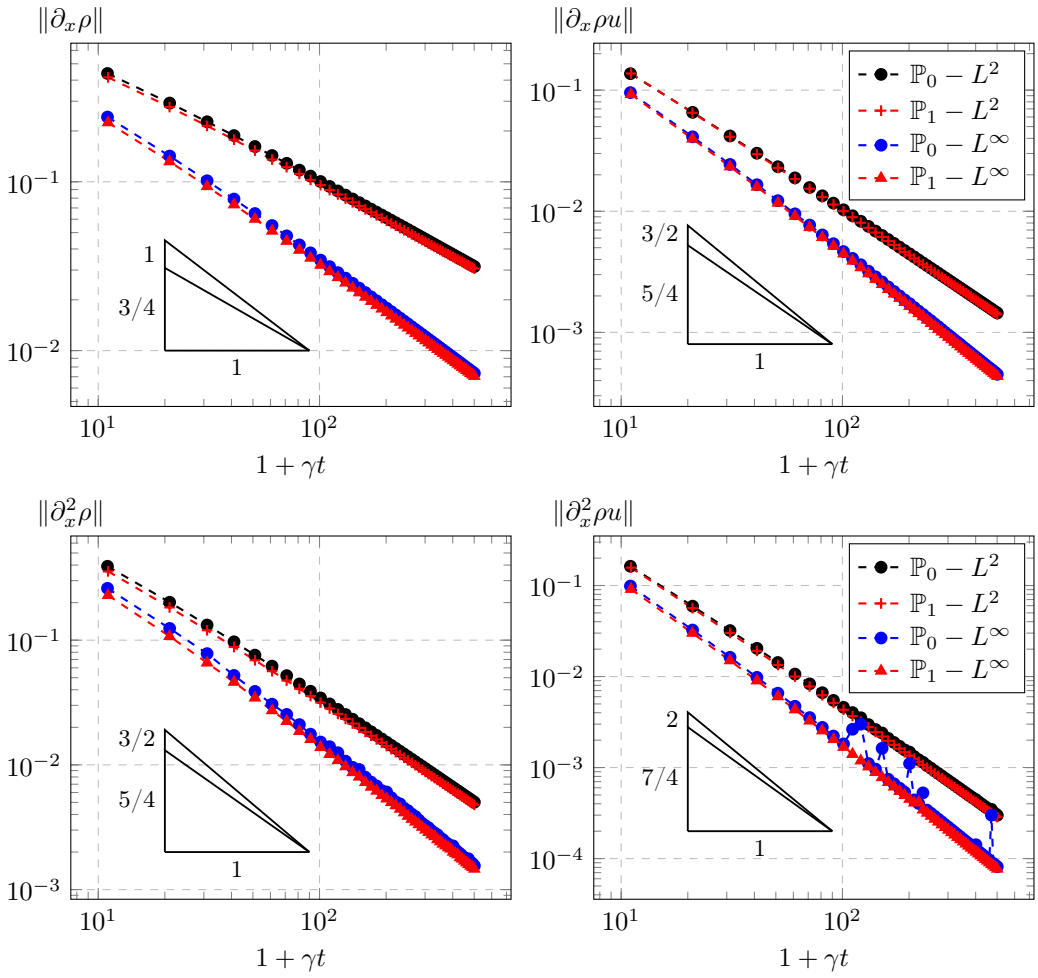

Figure C.22: Convergence speeds to the equilibrium in L^2 and L^∞-norms for the space derivatives of the density and momentum with $\Delta x = 5 \times 10^{-2}$ and $\kappa = 5$ in 1D